Reducing the water usage of post-combustion capture systems: the role of water condensation/evaporation in rotary regenerative gas/gas heat exchangers

Reducing the water usage of post-combustion capture systems: the role of water condensation/evaporation in rotary regenerative gas/gas heat exchangers

Laura Herraiz[a,*], Dougal Hogg[b], Jim Cooper[b], Mathieu Lucquiaud[a]

[a]*The University of Edinburgh, School of Engineering, The Kings Buildings, Edinburgh EH9 3JL, United Kingdom*
[b]*Howden Global, Old Govan, Renfrew, PA4 8XJ, United Kingdom*

* Corresponding author. Tel.: +44-131-650-7444;
E-mail address: l.herraiz@ed.ac.uk

Key words: Post-combustion carbon capture, water management, combined cycle gas turbine, dry cooling, rotary regenerative heat exchanger, exhaust gas recirculation.

Abstract

Water usage is expected to greatly increase when CO_2 capture is added to thermal power plants. A major contribution is the reduction of flue gases temperatures from 100-150 ºC to 30-50 ºC. The majority of studies to date propose the use of direct contact cooling, combining a cold water loop with water cooling. This article expands on a previous study of the same authors [1] proposing dry air-cooled options with rotary regenerative gas/gas heat exchangers, relying on ambient air as the cooling fluid, to eliminate the use of process and cooling water prior to the carbon capture system. It proposes, for the first time, a new stand-alone model of a bi-sector air/gas rotary heat exchanger, which includes the contribution to heat transfer of condensation/evaporation when flue gases are cooled below the dew point. It shows that water condensation from the flue gases in one sector of the heat exchanger, enhances the total heat transfer rate, due to the diffusion of water through the non-condensable gases boundary layer. In order to maintain the cooling capacity of these rotary regenerative heat exchangers, initially designed to operate without condensation, this article shows that they should be designed with surface properties, gas velocities and heat transfer channel geometries with the aim of allowing water condensate to remain on the metal elements surface, and then evaporate into the air stream when the metal elements have rotated to the air side. The model also predicts the location of water condensation, so that enamelled elements can be incorporated to the cold-end tiers of metal elements and mitigate any possible long-term corrosion problems.

1. Introduction and background

The environmental impact of energy systems decarbonisation on freshwater sources and marine environment is of growing concern [2]. In industrialised countries, water abstraction for electricity production currently can constitute up to around 40% of the total abstraction from fresh water sources [3,4]. Water demand associated to electricity generation is expected to rise further in places due to electrification with new build thermal power plants and, even more, if decarbonisation of electricity generation takes place with high contribution of carbon capture and storage (CCS) technologies in fossil fuel power plants [5]. The potential impact of a low carbon electricity system with different generation portfolios on regional water stress have been assessed in many studies, some have quantified the future freshwater demands for different energy pathways in Europe [3,6–8], in the United States [9–11], in China [12] or the whole word [13]. The extent of the increase in water stress strongly depend on penetration level of carbon capture, installed power plant capacity and cooling water technologies [8].

Post-combustion carbon capture (PCC) using amine-based solvent technologies is a possible option for commercial scale deployment of CCS in fossil fuel power plants, e.g. Boundary Dam CCS project in Canada, in operation since 2014, and Petra Nova CO_2 capture project in the United States, which began operation in 2016. Chemical absorption with amine-based solvents currently require large cooling capacity for the exhaust flue gas entering the absorber, the water wash system, the absorber intercooler, the lean solvent cooler, the reflux reboiler duty and the CO_2 compression inter-stage coolers. Most of the cooling capacity comes from water abstraction from natural environments. Thus, the availability of cooling water might constitute a limitation for the full scale deployment of PCC, particularly in regions with increasing restricted access to cooling water and limited availability of fresh or sea water abstraction licenses e.g. Middle East, Western China, Parts of the USA, industrial regions in Europe with extensive water abstraction regulated by local authorities. A reduction in cooling water demand is possible by using alternative dry cooling systems, yet there are few studies that have further develop the technical concept [5]. This article expands on a previous study of the same authors [1] proposing dry air-cooled options.

A feasibility study of a series of technology options with rotary regenerative gas/gas heat exchangers conducted by Herraiz et al. [1] shows that it is possible to greatly mitigate the increase of water usage associated with the addition of carbon capture to fossil fuel power generation. Rotary regenerative heat exchangers indirectly transfer heat by convection as a high heating capacity medium rotates and is periodically exposed to hot gas and cold gas streams, flowing in a counter current arrangement [14]. The study is focused on the management of the water balance around the absorber of the capture process in combined cycle gas turbine (CCGT) plants for two power plants configurations: an air-based combustion CCGT plant and a CCGT plant with exhaust gas recirculation (EGR). EGR is the process of diverting a fraction of the combustion gases at the outlet of the heat recovery steam generation (HRSG) to the inlet of the compressor of the gas turbine (GT). It has been studied in literature as a strategy to increase the CO_2 concentration and reduce the volume of gases treated in the capture plant, with the objective of minimising investment and operational costs [15–17].

A hybrid cooling system and a dry cooling system are proposed [1] to replace the direct contact cooler (DCC) typically used in flue gas scrubbing technologies:

- Hybrid cooling configurations with a gas/gas heat exchanger upstream of the DCC reduce cooling and process water demand by 67% and 35% respectively compared to a wet cooling system where the flue gas is primarily cooled in a larger DCC. Heat is transferred from the exhaust flue gas leaving the HRSG into the CO_2-depleted gas leaving the capture plant. The CO_2-depleted gas stream is reheated in the gas/gas heat exchanger above 70 ºC with enough buoyancy to rise through the stack.

- Dry cooling configurations rely on ambient air as the cooling medium and eliminate the use of process and cooling water prior to the absorber maintaining the temperature of the flue gas entering the absorber at approximately 45 ºC. Dry cooling configurations consist of a gas/gas heat exchanger and an air/gas heat exchanger in series. The baskets containing the heating elements are 1.2 m and 1 m long and the casing diameters are approximately 15 m and 13 m, respectively. A more compact configuration is possible with a gas/gas/air heat exchanger with a trisector arrangement. The baskets containing the heating elements are 1.4 m long and the casing diameter is approximately 18 m.

The implementation of hybrid cooling and dry cooling systems in an air-based combustion CCGT plant and in a CCGT plant with EGR is presented in Figure 1 and Figure 2, respectively. The flow direction and the typical temperatures in a bi-sector and a tri-sector rotary heat exchanger are shown in Figure 3.

The exhaust flue gas leaving the HRSG is cooled down to an optimum temperature prior to entering the capture plant. For amine-based chemical absorption, the flue gas is typically cooled down to ca. 45 ºC, yet the temperature should be adapted to the specific solvent. The selection is generally a trade-off between reaction kinetics and thermodynamic equilibrium, i.e. a high temperature favours the kinetic reaction rate while a low temperature enhances the solvent capacity [18]. Dry cooling systems with rotary heat exchangers should therefore be able to operate at a range of cold end temperatures in order to allow for the use of a wide range of solvents and avoid lock-in to a specific solvent technology, i.e. first-of-a-kind capture plants should be able to be upgraded with advanced future solvents.

Rotary regenerative heat exchangers for heat recovery from hot flue gases typically operate at temperatures well above the dew-point. They have been widely used in coal fired power plants to preheat the primary and secondary combustion air streams using the flue gases exiting the boiler, and to recover heat from the inlet stream of flue gas desulphurization (FGD) systems to increase the temperature of the outlet stream and its buoyancy at the stack. Mathematical models developed in literature consider convection to be the only mechanism of heat transfer between the flue gas streams and the solid matrix [19–21].

If a flue gas temperature below the dew point is required for the capture process, i.e. lower than 45 ºC in an air-based CCGT plant at ambient pressure, or 50 ºC in a CCGT plant with EGR at 35% recirculation ratio, water condensation would occur and additional cooling capacity would be necessary to remove the latent heat of condensation. This could be achieved either by increasing the heating surface area or by operating with large cooling air flow rates. Ambient air conditions could also result in water condensation if, for instance, the ambient temperature was lower than the design temperature of 15 ºC, since the flue gases temperature at the cold end would also decrease.

Water vapour would condense on the surface of the metal elements in the flue gas section and the condensate would be transferred to the adjacent air section. A large fraction of water droplets could drop by gravity and some would evaporate in the air stream in an air/gas heat exchanger or in the CO_2-depleted gas stream in a tri-sector gas/gas/air heat exchanger, as illustrated in Figure 4. The amount of condensate which would remain on the surface of the metal elements would be the result of a force balance between the gravitational force, the shear forces exerted by the gases and the adhesive forces between the droplets and the condensation surface. These forces depend on the direction of the flow, the gas velocity and the wettability of the metal surface [22,23].

Rotary systems are also often used in heating, ventilation and air conditioning (HVAC) technologies, where the rotor contains a desiccant porous media matrix. The combined processes of cooling and dehumidification, and of heating and humidification of air streams require models describing simultaneous heat and mass transfer [20,24]. The mass transfer mechanism in enthalpy recovery wheels is sorption/ desorption, rather than condensation/ evaporation investigated here. Both mechanisms are

described with the same differential equations, yet different thermodynamic relationships are implemented [25].

This article expands on a previous study of the same authors [1] and it further investigates the use of rotary regenerative heat exchangers for the dry cooling of flue gases in CCGT plants equipped with PCC. A novel contribution of this work is a feasibility assessment of the operation of rotary regenerative heat exchangers for a wider range of cold-end temperatures, so that dry cooling systems can be integrated to any post-combustion capture technology. Particular attention is given to operation temperatures below the flue gas dew point resulting in water condensation on the heating elements, since these heat exchangers are conventionally designed for non-saturation conditions in coal-fired power plants. This is particularly important in a CCGT plant with EGR, since the water content in the flue gas and, hence, the saturation temperature increase at higher recirculation ratios. Modelling tools are developed here for the first time to assess the effect of water condensation and subsequent evaporation on the thermal performance of a bi-sector rotary heat exchanger. Options to enhance the flue gases cooling capacity of heat exchangers initially designed for non-saturation conditions are proposed.

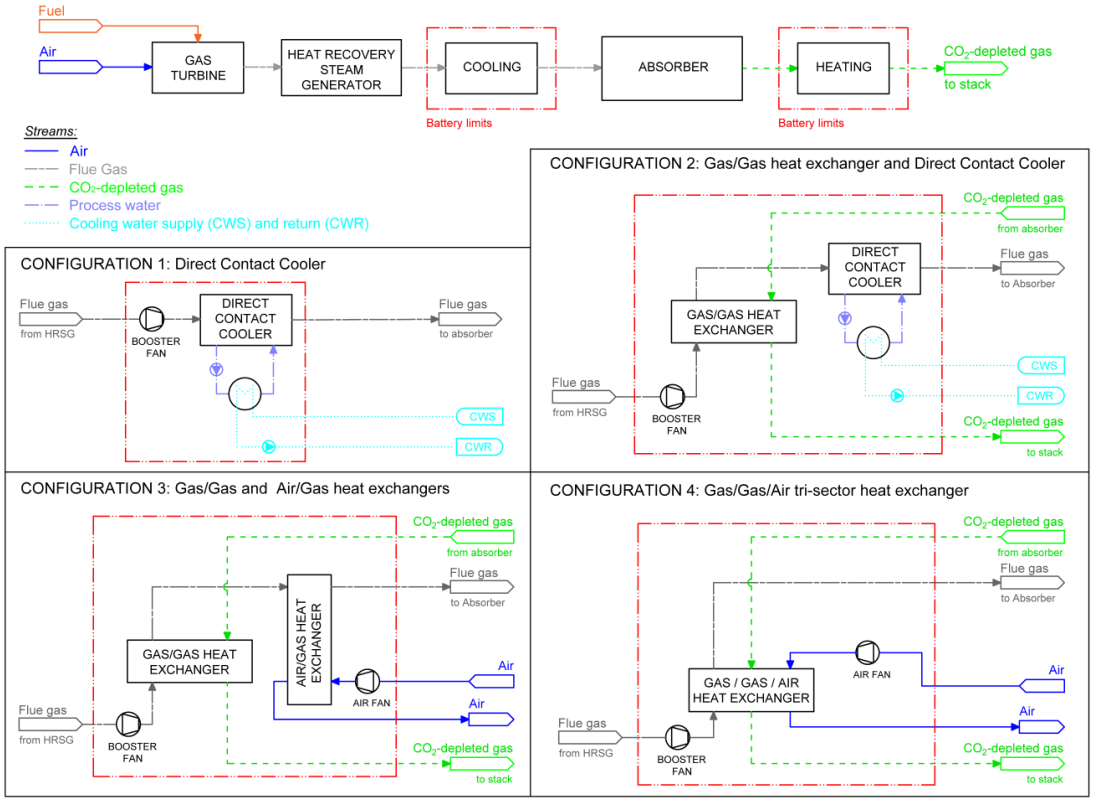

Figure 1.- Block flow diagram of rotary heat exchangers configuration for an air based combustion gas turbine combined cycle plant with post-combustion CO_2 capture [1]

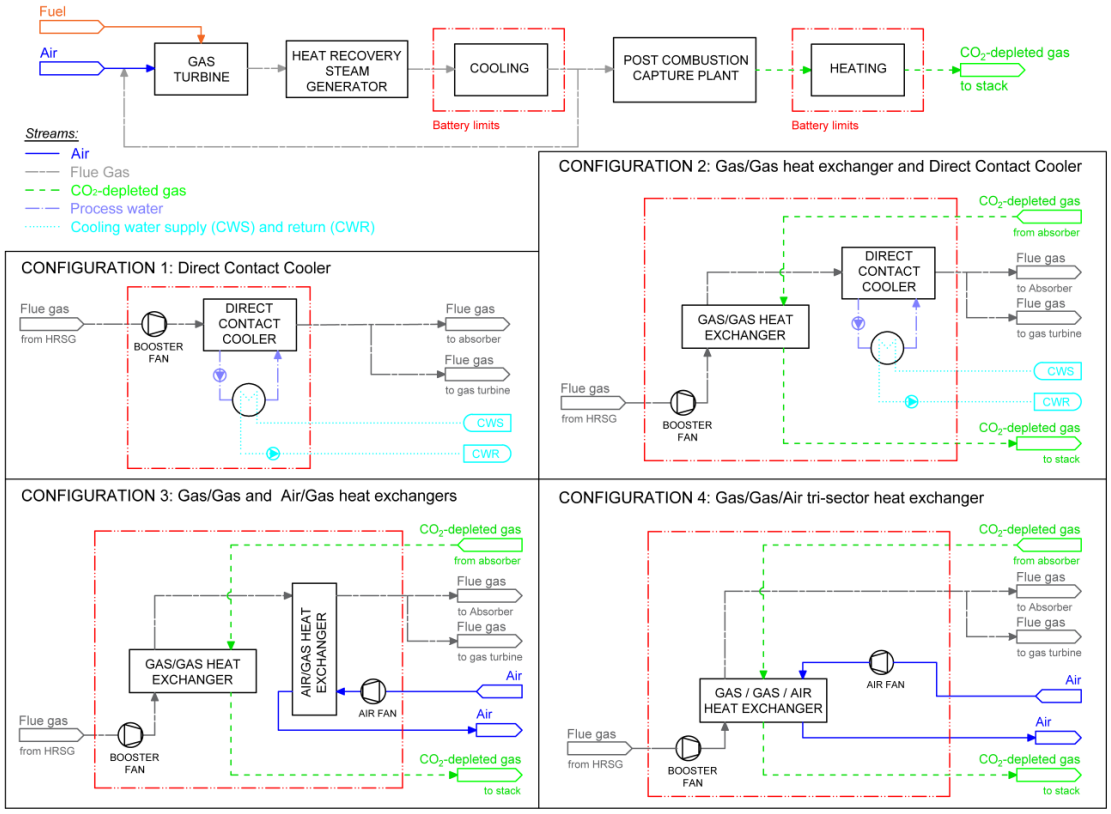

Figure 2.- Block flow diagram of rotary heat exchangers configuration for a gas turbine combined cycle plant with exhaust gas recirculation and post-combustion CO_2 capture [1]

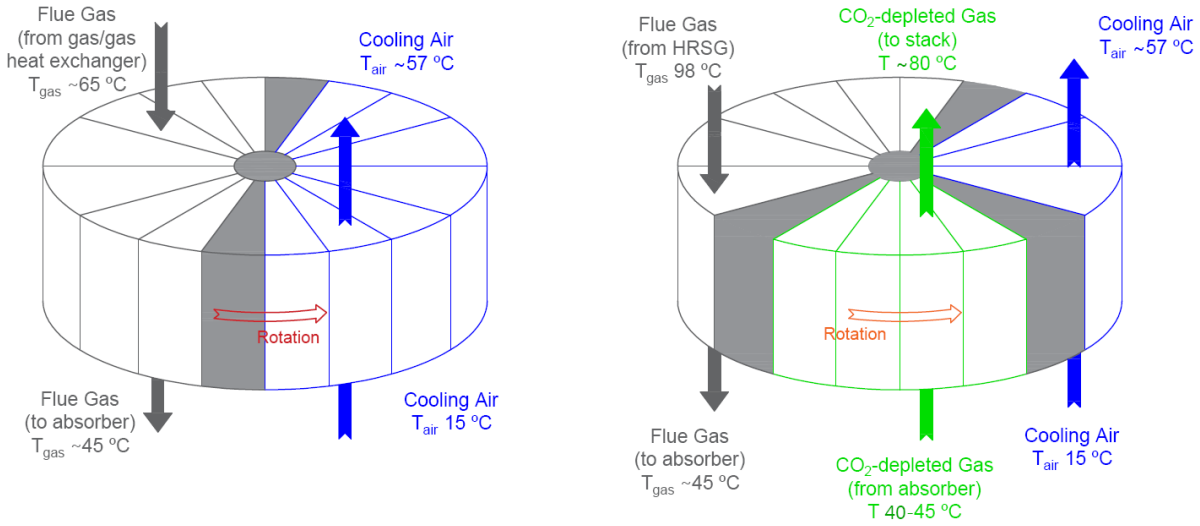

Figure 3.- Flow direction and typical temperatures of flue gas, CO_2 depleted gas and/or air in a bi-sector air/gas rotary heat exchanger (Configuration 3) and in a tri-sector gas/gas/air rotary heat exchanger (Configuration 4) (adapted from [1]).

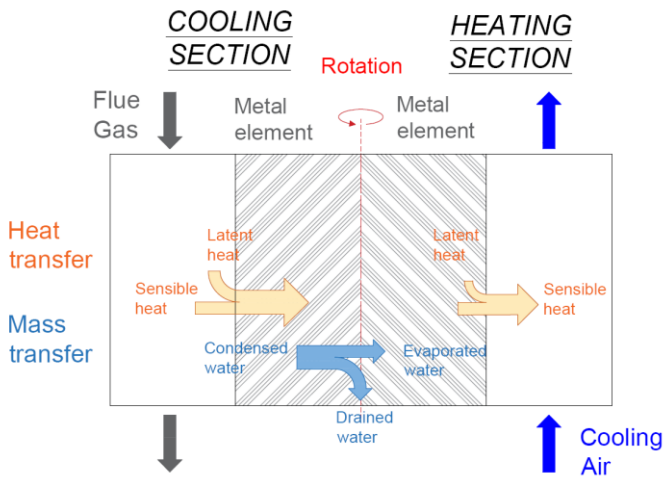

Figure 4.- Qualitative diagram of mass and heat transfer in the cooling and heating sections of an air/gas rotary regenerative heat exchanger with bi-sector configuration (adapted from [1]).

2. Theoretical analysis

Rotary regenerative heat exchangers indirectly transfer heat by convection as a heat storage medium continuously rotates and is periodically exposed to a hot and a cold gas stream with counter-current flow arrangement. The heat storage medium consists of a compact arrangement of pairs of specially formed metal plates packed into self-contained baskets installed into the rotor, providing very high surface area per unit volume [14].

The flue gas stream is cooled down when brought into contact with the metal elements in the cooling section. The metal elements absorb the heat and release it when they rotate and enter into contact with the cold gases, i.e. a CO_2-depleted gas and/or an ambient air stream, as illustrated in Figure 3. The temperature difference between the gas phase (T_G) and the solid surface (T_S) is the driving force for sensible heat transfer by forced convection, as illustrated in Figure 5a.

In the cooling section, condensation of water vapour occurs on the solid surface if the temperature of the metal elements is below the flue gas dew point temperature. The solid surface is then gradually wetted by the condensate and either a liquid film or liquid droplets are formed. The form of condensation, i.e. film-wise condensation or drop-wise condensation, depends on the wettability of the surface, which is a function of the free surface energy of the solid material and the surface tension of the condensing fluid [22,23]. The condensate is surrounded by a non-condensable gas boundary layer and the condensation of water vapour continues at the interface driven by the diffusion of vapour through the non-condensable gas layer. A large fraction of water droplets could drop by gravity and some would remain on the solid surface and evaporate into the air stream in the heating section of the rotary heat exchanger.

Flue gas condensation in natural gas fired boilers is considered as water vapour condensation in the presence of a large fraction of non-condensable gases, since the vapour concentration is in a range of 8 to 20 vol% [26,27]. The temperature and the vapour partial pressure distribution are presented in Figure 5b. There is a temperature drop through the non-condensable gas layer, from the bulk gas temperature (T_G) to the temperature at the gas-liquid interface (T_i), because the decrease of vapour concentration leads to lower partial pressure of vapour and then its saturation temperature is reduced. The water vapour pressure decreases from the partial pressure in the bulk gas (p_{H2Ov}) to the partial pressure at the interface ($p_{H2O\,i}$). According to previous studies, the condensate film is very thin and its thermal resistance is negligible. Thus, the solid surface temperature is equal to the temperature at the interface ($T_i \approx T_S$). The water vapour pressure at the interface is equal to the saturation pressure at the solid temperature ($p_{H2O\,i} \approx p_{H2O\,sat}$).

The temperature and the vapour pressure distribution for flue gas condensation are compared with that for convection heat transfer, illustrated in Figure 5a, and with that for condensation of pure vapour, illustrated in Figure 5c. In pure vapour condensation, it is important to note that the heat transfer is due to vapour condensation at the interface and the resistance to heat transfer comes from the condensed film. The bulk temperature (T_{vapor}) and the liquid-vapour interface temperature (T_i) are identical and equal to the saturation temperature of pure vapour (T_{sat}) [23].

Theoretical studies and experimental tests have been conducted in literature with the aim of recovering the latent heat from an exhaust flue gas stream in CCGT plants, using geometries of vertical or horizontal banks of tubes [26]. The two most widely followed approaches for the analysis of mass and heat transfer are a boundary layer analysis and a heat and mass analogy from the Colburn and Hougen theory.

The boundary layer analysis consists of solving the governing equations of the condensate film and the vapour-non condensable gas mixture regions with appropriate boundary layer approximations. Such level of detail is necessary when the resistance to the heat transfer exists mainly in the condensate film, which is the case of pure vapour condensation and vapor condensation in a gas mixture with a high concentration of water vapour [26,28].

The Colburn and Hougen method is most widely used when the non-condensable gases are dominant in volume, i.e. concentrations above 80 vol%. The condensation mass transfer is then controlled by the diffusion through the non-condensable gas layer, and the mass transfer rate is analogous to the heat transfer rate [26,27,29]. This method is considered in this work to develop the equations describing the heat and mass transfer rate, implemented in the stand-alone model of a bi-sector rotary heat exchanger described in Section 3.2.

At any section in the heat exchanger, the heat transfer rate is the sum of the sensible heat due to forced convection, and the latent heat due to vapour condensation in the gas side or water evaporation in the air side. The heat transfer rate is given by Equation (1), where $h_{overall}$ is the overall heat transfer coefficient, so called convection-condensation heat transfer coefficient, and dA is the area of an infinitesimal element at the outer side of the boundary layer. The heat transferred due to convection is calculated from Equation (2), where h_{cv} is the convective heat transfer coefficient, and the heat transfer due to condensation is evaluated from Equation (3), where h_{cond} is the condensation heat transfer coefficient. The condensation heat transfer rate can also be written in terms of the latent heat of condensation (h_{fg}) and the mass flow rate of the condensate $(d\dot{m}_{cond})$. The overall heat transfer coefficient is therefore the sum of the convection heat transfer coefficient and the condensation heat transfer coefficient, as indicated in Equation (4), since the resistances to heat transfer are in parallel.

$$d\dot{Q} = d\dot{Q}_{convection} + d\dot{Q}_{condensation} = h_{overall} \cdot (T_G - T_S) \cdot dA \tag{1}$$

$$d\dot{Q}_{convection} = h_{cv} \cdot (T_G - T_S) \cdot dA \tag{2}$$

$$d\dot{Q}_{condensation} = h_{cond} \cdot (T_G - T_S) \cdot dA = h_{fg} \cdot d\dot{m}_{cond} \tag{3}$$

$$h_{overall} = h_{cv} + h_{cond} \tag{4}$$

The heat transfer is accompanied by mass transfer due to water condensation or evaporation. The mass flow rate of condensate can be expressed in terms of the mass transfer coefficient (h_m), and the difference between the molar fraction of vapour in the bulk gas $(y_{H2O,v})$ and at the interface $(y_{H2O,i})$, as illustrated in Equation (5). The driving force for mass transfer can also be written in terms of partial pressures, where $p_{H2O,v}$ is the water vapour pressures in the bulk gas and $p_{H2O,sat}$ is the saturation pressure at the solid temperature. According to the Colburn-Hougen analogy, explained in Appendix E, the mass transfer coefficient can be obtained from Equation (6), where h_{cv} is the convection heat transfer coefficient, ρ_G is the density of the gas phase, Sc is the Schmidt number and Pr is the Prandtl number.

$$d\dot{m}_{cond} = h_m \left(y_{H2O,v} - y_{H2O,i}\right) \cdot dA = h_m \cdot MW \left(\frac{p_{H2O,v}}{R \cdot T_G} - \frac{p_{H2O,sat}}{R \cdot T_S}\right) \cdot dA \tag{5}$$

$$\frac{h_{cv}}{h_m} = \rho_G \cdot C_{p\,G} \cdot \left(\frac{Sc}{Pr}\right)^{2/3} \tag{6}$$

Theoretical models and experimental data are combined to develop correlations for the Nusselt and Sherwood numbers, which are used to evaluate the heat and mass transfer coefficients. The empirical correlations reported in the open literature for water condensation in the presence of non-condensable gases are obtained under certain experimental conditions and for a specific geometry. They are therefore only valid within a range of water vapour mass fractions and Reynolds numbers, and for external flow around vertical or horizontal tubes [27,29,30].

Due to the lack of experimental work for condensation heat transfer in rotary heat exchangers, the theoretical analysis conducted by Liang et al. [29] is considered here as reference to obtain the correlation of the overall heat transfer coefficient implemented in the stand-alone model of a rotary heat exchanger. As explained in more detail in Appendix D, the analysis leads to a dimensionless parameter group known as the *augmentation factor*, which takes into account the effect of the condensation of a relatively small amount of water vapour on the convection heat transfer. The Nusselt number for convection heat transfer (Nu_{cv}), shown in Equation (7), is multiplied by the augmentation factor to obtain a normalized correlation of the Nusselt number for convention-condensation heat transfer coefficient, presented in Equation (9). The Nusselt number for condensation heat transfer is given in Equation (8). Experimental results show that the convection-condensation heat transfer coefficient increases with the Reynolds number and the bulk vapour mass fraction, and it is approximately 1 to 4 times that of the forced convection heat transfer without condensation [27,29].

$$Nu_{cv} = C \cdot Re^{m} \cdot Pr^{1/3} \tag{7}$$

$$Nu_{cond} = C \cdot Re^{m} \cdot Pr^{1/3} \cdot \left(Le^{-2/3} \cdot B \cdot Ja^{-1}\right) \tag{8}$$

$$Nu_{overall} = Nu_{cond} + Nu_{cv} = C \cdot Re^{m} \cdot Pr^{1/3} \cdot \left(1 + Le^{-2/3} \cdot B \cdot Ja^{-1}\right) \tag{9}$$

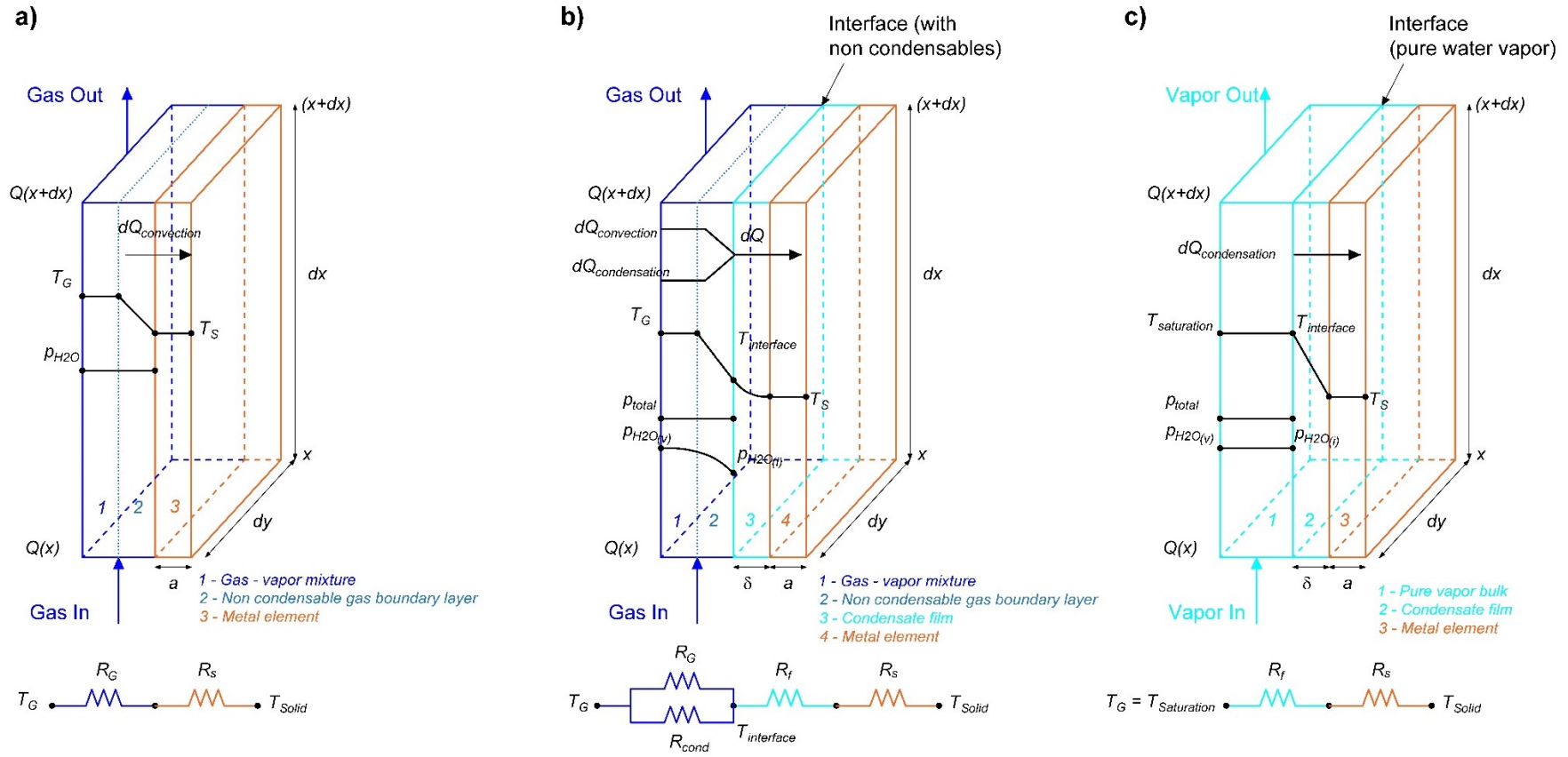

Figure 5.- Boundary layer temperature and pressure distributions for the cooling process of a gas stream (a), and for the process of cooling and water condensation in a gas stream with a large concentration of non-condensable gases (b), and a pure water vapour stream (c).

3. Modelling methodology

3.1 Operation conditions for condensation in flue gases from n plants

The operation conditions leading to water condensation on the metal elements of the rotary heat exchanger are first identified, by conducting sensitivity analysis for two configurations of gas-fired power plants: an air-based combustion CCGT plant and a CCGT with exhaust gas recirculation. The description of the reference CCGT plant, as well as the composition, the flow rates and the temperature of the flue gases leaving the HRSG for a range of recirculation ratios are provided in Appendix A.

- For an air-based combustion CCGT plant, the contribution of the latent heat transfer to the total heat transfer rate and the amount of condensed water in the exhaust flue gases are evaluated for a range of temperatures at the cold-end of the rotary heat exchanger from 30ºC up to 50ºC.
- For a CCGT plant with EGR, the contribution of the latent heat transfer and the amount of condensed water are first evaluated for a range of recirculation ratios from 0 to 50%, considering that the flue gas is cooled down to 40ºC, and then for a range of temperatures at the cold-end of the rotary heat exchanger from 30 ºC up to 50ºC at 40% recirculation ratio.

To conduct the sensitivity analysis, the overall energy and mass balances around the dry-cooling system are solved, assuming that the flue gases leave the heat exchanger saturated in moisture at the cold-end temperature. Is it also assumed that the condensed water remains on the surface of the metal elements and is completely evaporated into the air in the heating section of the bi-sector rotary heat exchanger.

3.2 Process modelling of a of a bi-sector rotary heat exchanger

To assess the operational feasibility of rotary heat exchangers for dry cooling of the flue gases at temperatures below the dew point, the effect of water vapour condensation, and subsequent evaporation, on the thermal performance of a rotary heat exchanger is further investigated through process modelling.

A stand-alone model of a bi-sector air/gas rotary heat exchanger is built in gPROMS Model Builder, a process modelling software that allows to create customized models. The property method of Peng-Robinson as equation of state for gas, and the Steam Tables (IAPWS-95) for water/steam are selected in Multiflash; the standard gPROMS physical properties package [31].

The mathematical model that accounts for convection-condensation heat transfer consists of a system of partial differential equations that describe the sensible heat transfer, due to forced convection, and latent heat transfer, due to vapour condensation or water evaporation. The sensible heat transfer is written as the enthalpy change of the gas stream. The latent heat transfer can be written in terms of condensation/evaporation flow rate. The amount of energy lost/gained by the fluid is equal to the amount of energy gained/lost by the metal elements. The energy balance is written as indicated in Equation (10) and Equation (11), where T_S is the metal elements temperature, T_G is the gas/air temperature, $\dot{n}_G$ is the gas/air molar flow rate, $\dot{n}_{H2O,G}$ is the molar flow rate of water vapour in the gas/air stream, m_S is the total mass of the metal elements, $C_{p\,G}$ and $C_{p\,S}$ are the heat capacity of the gas and the solid respectively, h'_{fg} is the latent heat of condensation/evaporation and A_s is the total surface heating area of the metal elements.

$$\dot{n}_G \cdot C_{p\,G} \cdot \left(\frac{\partial T_G}{\partial x}\right) + h'_{fg}\left(\frac{\partial \dot{n}_{H2O,G}}{\partial x}\right) = h_{overall}\ \frac{A_s}{L}(T_S - T_G) \quad (10)$$

$$m_S \cdot C_{p\,S} \cdot \frac{1}{L} \cdot \left(\frac{\partial T_S}{\partial \tau}\right) = h_{overall}\ \frac{A_s}{L}(T_G - T_S) \quad (11)$$

The resistance through the condensed phase can be neglected due to the large volume of non-condensable gases in the flue gas stream, and it occurs only in the non-condensable gas boundary layer. The overall heat transfer coefficient, $h_{overall}$, accounts therefore for the convection heat transfer coefficient , h_{cv}, and the condensation heat transfer coefficient, h_{cond}, as explained in Section 2. The correlation of the Nusselt number implemented in the gPROMS model to obtain the overall heat transfer coefficient is shown in Equation (9). The theoretical analysis conducted to obtain this correlation is presented in Appendix D.

Heat transfer is accompanied by mass transfer of water vapour through the non-condensable gases boundary layer, described by Equation (12), where $\dot{n}_{H2O,G}$ is the molar flow rate of water vapour in the gas/air stream, $y_{H2O,G}$ and $y_{H2O,i}$ are the molar fractions of water vapour in the bulk gas/air and at the interface respectively, and h_m is the mass transfer coefficient. The mass transfer coefficient is evaluated as a function of the convection heat transfer coefficient, h_{cv}, according to the heat and mass transfer analogy shown in Equation (6), obtained from the Colburn and Hougen theory as explained in Appendix E.

$$\left(\frac{\partial \dot{n}_{H2O,G}}{\partial x}\right) = h_m\ \frac{A_s}{L}\left(y_{H2O,G} - y_{H2O,i}\right) \quad (12)$$

The system of partial differential equations is solved by finite difference approximations and boundary conditions. The mathematical model as implemented in gPROMS for only convective heat transfer and for both convective and condensation heat transfer is described in Appendix B and Appendix C respectively, for a rotary heat exchanger with a bisector arrangement. The system domain is discretised into $N_L x N_\tau$ stages, as illustrated in Figure 6b, where N_L is the number of stages in longitudinal direction and N_τ is the number of stages in angular direction. The temperature, the composition, the flow rate, and the thermal and physical properties of the flue gas and air streams are continuous variables along the axial direction (x) and the angular direction (τ), yet they are evaluated in each stage (s,j) in the discretised system. The following assumptions are considered for the development of the model:

a) Steady state. After a number of cycles the temperature variation at all points along the rotary heat exchanger become independent of the initial temperature distribution. When this occurs, the heat exchanger achieves cyclic equilibrium and steady state conditions.

b) Two dimensional axial symmetric flow. The properties of the gases and the solid vary along the axial and angular direction, yet they are assumed constant along the radial direction.

c) Adiabatic system. The heat loss to or heat gain from the surroundings/environment through the walls of the rotary heat exchanger is negligible.

d) Uniform and constant inlet conditions. The inlet velocity and the temperature of the gas streams are uniform over the flow cross section and constant with time.

e) Resistance to heat transfer through the condensate film is neglected, which can be assumed for gas-vapour mixtures with more than 80 vol% of non-condensable gases.

f) The hot and cold gases flow in a counter-current arrangement. The contacting mode of the gas and the metal elements is cross-flow.

g) At the interface between the gas and the condensate phase, the gas is saturated in water vapour.

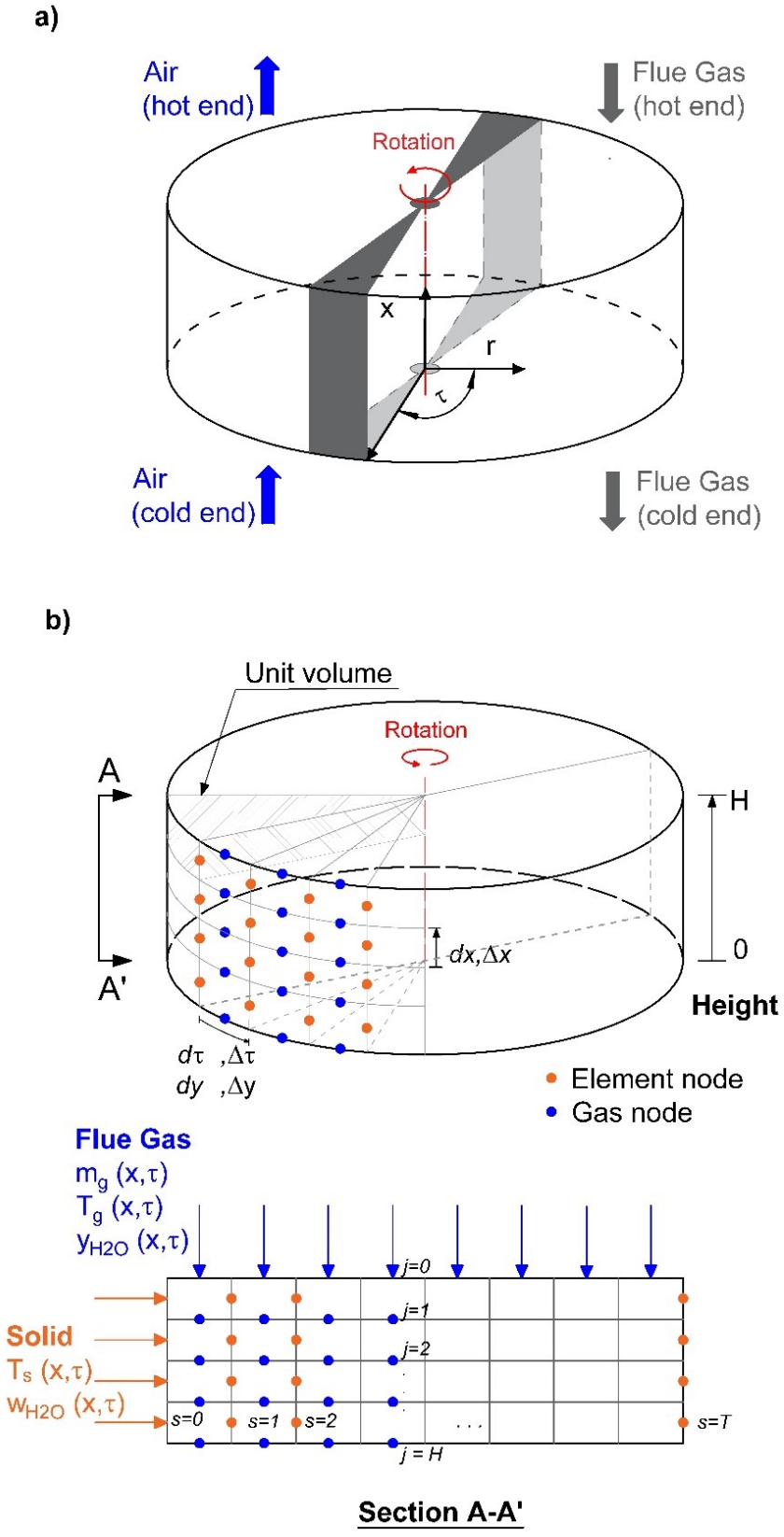

Figure 6.- (a) Schematic representation and (b) Discretized domain of the rotary heat exchanger.

Process modelling is conducted for the air/gas rotary heat exchanger of a dry-cooling system consisting of two consecutive rotary heat exchangers in series (see Configuration 3 in Figure 1 and Figure 2), which replace the direct contact cooler of the convectional wet cooling system. The first gas/gas heat exchanger transfers sensible heat from the exhaust flue gas stream to the CO_2-depleted gas stream to reach the temperature necessary for adequate buoyancy at the inlet of the stack. The flue gas temperature is then further reduced in an air/gas heat exchanger using ambient air as the cooling fluid. If the flue gas is cooled down below the saturation temperature in the air/gas heat exchanger, water vapour condensation and subsequent water evaporation may occur, and both sensible and latent heat will be transferred. The air/gas heat exchanger is modelled in this work to investigate the effect of water condensation/evaporation on the thermal performance. The design parameters required for the gPROMS model are presented in Table 1.

- For an air-based combustion CCGT plant, the flue gases are first cooled down to the saturation temperature, i.e. approximately 45 ºC, so that only sensible heat is transferred from the flue gases to the air. The gPROMS model is validated for convective heat transfer in this configuration using Howden's proprietary software, which is used for thermodynamic analysis and the sizing of rotary heat exchangers in commercial scale applications. For this purpose, the gas temperature profile, the metal temperature profile and the heat transfer rate predicted by the gPROMS model are compared to those obtained by Howden's proprietary software.

- For a CCGT plant with EGR at 35% recirculation ratio, an air/gas heat exchanger, with the design parameters shown in Table 1, is used to cool down the flue gases to 45 ºC, which is below the gas dew point and water condensation is expected on the metal elements. The inlet stream variables are shown in Table 2.

An uncertainty of the model is the consideration of the fraction of condensed water that drains due to gravitational forces and the fraction that remains on the surface of the metal elements and evaporates into the air stream. The process modelling is conducted first assuming that all the condensed water remains on the surface of the metal elements and is evaporated into the air stream, and then assuming that all the condensed water drains and no water remains on the surface. The effect of both assumptions on the cooling capacity of the heat exchanger are compared. Results from the gPROMS model are presented in Section 4.2 in terms of the temperature, the condensed water flow rate and the heat transfer rate profiles.

In rotary heat exchangers, direct and entrained leakages may occur from a high CO_2 concentration stream to a stream with lower CO_2 concentration due to the pressure difference at both sides of the sector plate and due to rotation. Previous work by Herraiz et al. [1] estimates that leakage levels of ca. 0.5%-1% can be reasonably expected, although it would be possible to engineer purge and scavenge systems to minimise leakage flow rates even further [20,32].

The sensitivity analysis conducted shows that these conservative estimates of leakage rates could be tolerated and are likely to be deemed acceptable since they would only have a limited impact on the capture rate and on the operation of the post-combustion capture plant. The overall CO_2 removal rate for a range of leakages level is illustrated in Figure 7. It shows that for values lower than 1%, there is a marginal reduction of the overall CO_2 removal rate, approximately 0.45% for a leakage level of 0.5% for an absorber designed for a 90% removal rate.

It is also important to note that leakage levels lower than 3% do not have any significant impact on the thermal performance analysis of the rotary heat exchanger. In this work, the leakage flow rate

from the flue gas to the air stream is considered in the energy and mass balance to correct the temperature and composition of the gas streams leaving the heat exchanger.

Table 1.- Design parameters of the air/gas rotary heat exchanger

Configuration	--	Bi-sector
Diameter (inside rotor housing)	m	13
Height (metal elements length)	mm	1000
Front area	m^2	120
Heating surface area (single sided)	m^2	22985
Specific heat surface area	m^2/m^3	191
Sector splits	--	Gas 22.50, Air 20.50
Rotation speed	rpm	1

Table 2.- Inlet stream variables for the air/gas rotary heat exchanger for a CCGT plant with EGR at 35% recirculation ratio

Inlet streams:		**Air**	**Flue gases**
Pressure	kPa	101.3	111.3
Temperature	ºC	15	65
Mass flow rate	kg/s	350	638
MW	mol/g	28.84	28.36
Composition			
CO_2	%mol	0.03	6.55
H_2O	%mol	1.01	10.92
N_2	%mol	77.30	74.26
O_2	%mol	20.74	7.38
Ar	%mol	0.93	0.89

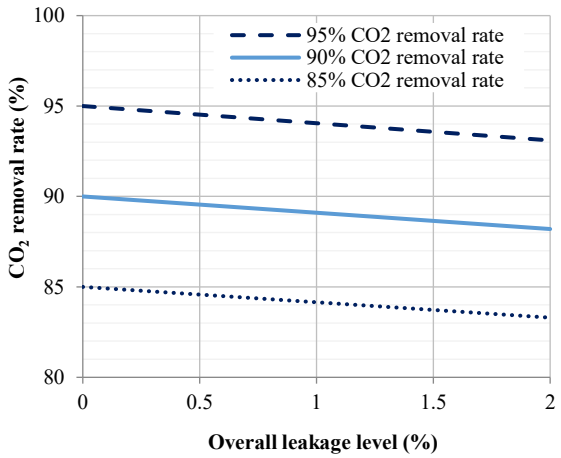

Figure 7.- Sensitivity of the overall CO_2 removal ratio to leakage level from the untreated flue gas into the CO_2-depleted gas [1]

4. Results and discussion

4.1 Sensitivity analysis

4.1.1. Air-based combustion Combined Cycle Gas Turbine plant

Water condensation on the heating elements occurs when the flue gas from a natural gas fired combined cycle plant is cooled down below ca. 45 ºC. The flue gas contains ca. 8.8 vol% water vapour, which corresponds to a saturation temperature of 45.5 ºC at 1.113 bar.

The amount of condensed water and the contribution of the latent heat to the total heat transfer rate increases for a lower flue gas temperature at the outlet of the air/gas heat exchanger. The contribution of the latent heat transfer (44%) is approximately the same as the contribution of the sensible heat transfer (56%) when the flue gas is cooled down to 35 ºC. Additional cooling capacity would therefore be necessary to remove the latent heat of condensation, which could be achieved either by increasing the heating surface area or by operating with large cooling air flow rates.

A sensitivity analysis of the convective and condensation heat transfer rate and the amount of condensed water to the flue gas temperature at the cold end of the air/gas heat exchanger is shown in Figure 8, for an air-based combustion CCGT power plant.

4.1.2. Combined Cycle Gas Turbine plant with exhaust gas recirculation

In a CCGT plant with exhaust gas recirculation (EGR), the water vapour concentration in the exhaust flue gases increases for high recirculation ratios, since the absolute humidity of the recycled flue gas stream is higher than that of the ambient air used for combustion. A water vapour content of 11 vol% is possible for a 35% recirculation ratio. Yet the water content depends on the temperature of the recycled flue gas, since, below the saturation temperature, condensed water is removed before entering the compressor of the gas turbine. The flue gas saturation temperature varies between 45.5 ºC, without EGR, and 51 ºC, at 40% recirculation ratio and 1.113 bar.

A sensitivity analysis of the convective and condensation heat transfer rates and the amount of condensed water to the water concentration in the flue gas is shown in Figure 9. The range of water concentrations in Figure 9 corresponds to a range of recirculation ratios (EGR ratio) from 0 to 50%, when both the recycled and non-recycled flue gas streams are cooled down to 40 ºC. For a CCGT plant with EGR at 40% recirculation ratio, a sensitivity analysis of the heat transfer rates and the amount of condensed water to the flue gas temperature at the outlet of the air/gas heat exchanger is presented in Figure 10.

If the flue gas of a CCGT with EGR needs to be cooled down below the saturation temperature prior entering the capture plant, the significant contribution of the latent heat to the overall heat transfer rate indicates that the effect of water condensation and subsequent evaporation have an important effect on the thermal performance and the design of an air/gas rotary heat exchanger. A large fraction of water droplets could drop by gravity and some could evaporate into the air stream in the heating section, as illustrated in Figure 4. The effect of the fraction of condensed water that drains off the system if therefore further investigated in Section 4.2.

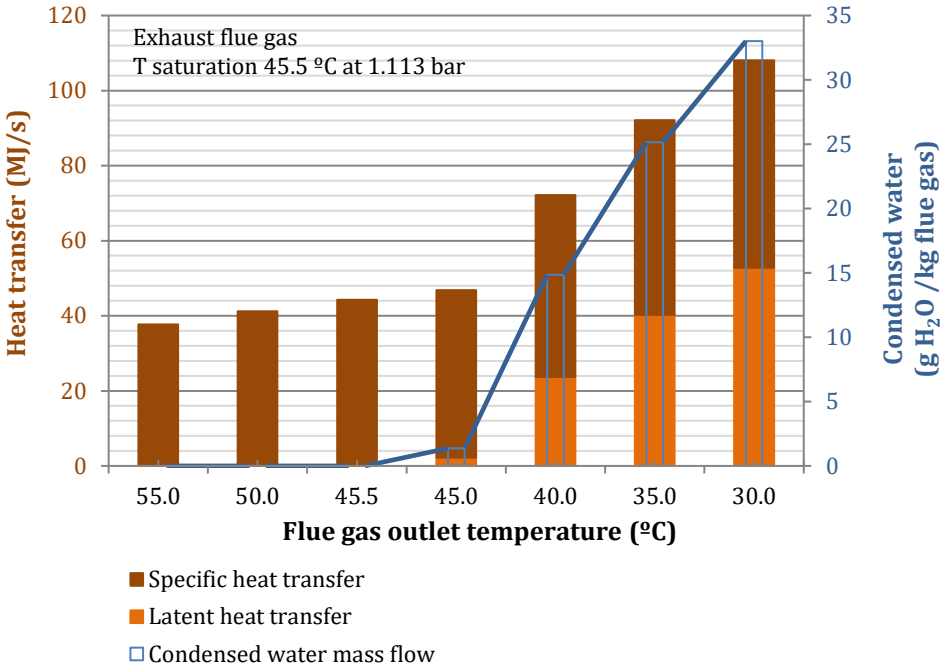

Figure 8.- Sensitivity of the sensible and latent heat transfer rates and the relative amount of condensed water to the flue gas temperature at the outlet of the rotary heat exchanger in an air-based combustion CCGT plant.

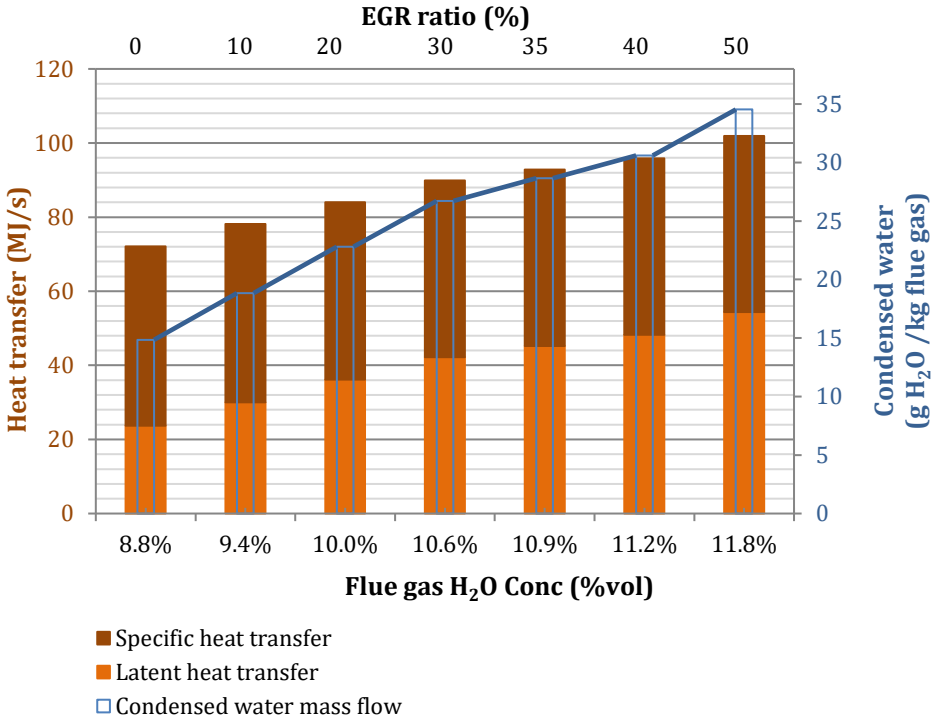

Figure 9.- Sensitivity of the sensible and latent heat transfer rates and the relative amount of condensed water to the water content in the flue gases of a CCGT plant with exhaust gas recirculation, for a recirculation ratio range from 0 to 50% (the flue gas is cooled down to 40 ºC).

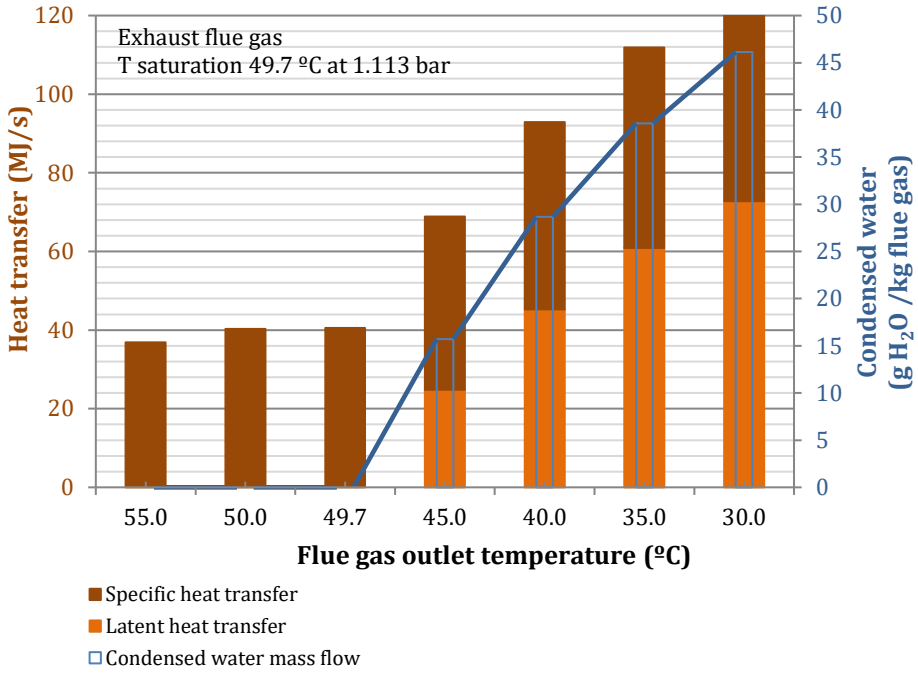

Figure 10.- Sensitivity of the sensible and latent heat transfer rates and the relative amount of condensed water to the flue gas temperature at the outlet of the rotary heat exchanger in a CCGT plant with exhaust gas recirculation at 35% recirculation ratio.

4.2 Thermal performance analysis of an air/gas rotary heat exchanger with condensation

The effect of water condensation on the thermal performance is further investigated in this section for the air/gas rotary heat exchanger of a dry cooling configuration, consisting of two rotary heat exchangers in series (see Configuration 3 in Figure 2). The exhaust flue gas from a CCGT plant with EGR at 35% recirculation ratio is cooled down to ca. 43 ºC. It is below the dew-point temperature of ca. 49.7 ºC at 1.113 bar. Water is therefore expected to condense on the surface of the heating elements at some locations of the heat exchanger. A recirculation ratio of 35% is considered here since it results in an oxygen concentration of approximately 17 vol% in the gas turbine combustor, which is the limiting oxygen level experimentally determined for GE F-class gas turbine engines to ensure stable flames and complete combustion, with acceptable levels of NOx, CO and unburned hydrocarbons emissions [15].

The flue gas stream leaving the HRSG is first cooled down from 98 ºC to 65 ºC in a gas/gas heat exchanger, where sensible heat is transferred to the CO_2-depleted gas coming from the absorber, raising its temperature to ca. 80 ºC, for adequate buoyancy at the stack. The flue gas is then further cooled down to ca. 43 ºC in an air/gas heat exchanger using ambient air as the cooling fluid. The air mass flow rate is 350 kg/s. The size optimisation and design of the rotary heat exchangers is conducted in a previous study of the same authors [1]. The gas/gas heat exchanger has a surface area of ca. 66000 m^2, and the rotor containing the heating elements is 1.22 m long and 15 m diameter (inside rotor housing). The air/gas heat exchanger has a surface area of ca. 46000 m^2, and the rotor is 1 m long and 13 m diameter (inside rotor housing).

Process modelling is conducted for the air/gas rotary heat exchanger, whose design parameters, as implemented in the gPROMS model, are presented in Table 1. To understand the uncertainty of the model in the evaluation of the fraction of condensate that remains on the metal elements, two approaches are considered

- The *convection-condensation heat transfer with water evaporation* approach assumes that all the condensed water remains on the surface of the metal elements and is completely evaporated into the ambient air stream as the elements rotate.
- The *convection-condensation heat transfer with water drainage* approach assumes that the condensed water completely drains off the system as it condenses.

Results are presented and compared hereinafter in terms of the temperature profiles of the flue gas and air streams in axial and angular dimensions, and the water condensation and evaporation flow rate profiles, in order to show the location in the rotary heat exchanger where water condensation is likely to occur. The metal elements temperature distribution and values of the augmentation factor, defined as the ratio of the convective-condensation heat transfer coefficient to the convective heat transfer coefficient, are included in Appendix F. The augmentation factor provides insight of the lower heat transfer resistance through the non-condensable boundary with simultaneous sensible heat and latent heat transfer. The augmentation factor is therefore higher than one at the locations where condensation or evaporation occurs.

Table 3.- Mean temperatures in the air/gas heat exchanger (gPROMS model)

Heat transfer mechanisms		***Convection - condensation***	***Convection - condensation***
Drain water fraction	**%**	**0**	**100**
Gas inlet temperature	ºC	65	65
Air inlet temperature	ºC	15	15
Gas outlet temperature	ºC	43.5	47.0
Air outlet temperature	ºC	50.5	51.7
Air side effectiveness	%	71	73
Gas side effectiveness	%	43	36
Metal temperature – Cooling section inlet	ºC	46	49
Metal temperature – Heating section inlet	ºC	48	50
Metal temperature – Hot end	ºC	56	57.7
Metal temperature – Cold end	ºC	36	43.6

4.2.1 Convection-condensation heat transfer with water evaporation

The flue gas is cooled down as it enters into contact with the metal elements. Heat is stored in the form of sensible heat and it is released as the elements rotate and enter into contact with ambient air. The temperature difference between the gas stream and the metal is the driving force for sensible heat transfer by convection. The flue gas temperature decreases from 65 ºC to 43.5 ºC and the air temperature increases from 15 ºC to 51.5 ºC, as presented in Table 3. Figure 11 shows the temperature profiles of the flue gas and air stream.

At some locations of the rotary heat exchanger, the metal temperature is lower than the flue gas dew point and the water vapour in the flue gas condenses. Water vapour diffuses through the non-

condensable gas boundary layer and condenses on the surface of the metal elements in the gas cooling section, remaining on the surface as they rotate. Water is completely evaporated into the ambient air stream in the heating section. Figure 12 shows the condensed water flow rate from the flue gas and the evaporated liquid water flow rate into the ambient air.

The total heat transfer rate corresponds to sensible heat transfer and latent heat transfer in the locations at which water condensation/evaporation occurs. A larger amount of heat needs to be removed from the flue gases, yet the overall heat transfer coefficient increases by a factor, known as augmentation factor, compared to the convection heat transfer coefficient. The resistance to heat transfer through the boundary layer is, therefore, smaller. The augmentation factor at different locations in the rotary heat exchanger is shown in Figure F.4.

4.2.2 Convection-condensation heat transfer with water drainage

The condensed water would drain off the heat exchanger as it condenses in the cooling section for certain operation conditions, e.g. high flue gas velocities, downward flow direction, and for certain surface properties of the metal and coating used for the heating elements manufacturing, e.g. low wettability of the surface. There would be no water remaining on the elements surface to be evaporated into the ambient air in the heating section, which results in a lower cooling capacity of the metal elements. The temperature profiles of the flue gas and the air streams are shown in Figure 13, and the condensed and evaporated water flow rates at different locations in the heat exchanger are presented in Figure 14.

The flue gas and air mean outlet temperatures for 100% and 0% water drainage are presented in Table 3. When condensed water drains off the heat exchanger, the metal elements enter the flue gas cooling section at a higher temperature, i.e. 49 ºC compared to 46 ºC for 0% drainage factor and full evaporation of condensed water into the ambient air. The lower cooling capacity results in a higher flue gas outlet temperature, i.e. 47 ºC compared to 43.5 ºC. This is due to the fact that, in the air heating section, the total heat transfer rate from the metal elements to the ambient air is smaller, since the only component is sensible heat and there is no additional heat removed due to water evaporation. Moreover, the resistance to heat transfer through the non-condensable boundary layer is higher, since the overall heat transfer coefficient corresponds to the convective heat transfer coefficient and the augmentation factor has therefore a value of one, as presented in Figure F.8.

In order to enhance the cooling capacity of a new-build rotary heat exchanger with water condensation, or to maintain the cooling capacity of an existing rotary heat exchanger initially designed to operate above the flue gas dew temperature, operating conditions and materials should be selected so that the condensed water remains on the surface of the heat elements as they rotate. Upward flow and low flue gas velocity is preferable to avoid liquid droplets carry-over. Moreover, an appropriate material selection and surface coating should aim at high wettability of the surface. Enamelled heating elements would be applied on the cold-end tiers of metal elements to mitigate any possible long-term corrosion problems, in a similar manner to flue gas desulfurization rotary heat exchanger applications.

x/L	GAS INLET												AIR OUTLET									
0.00	65.0	65.0	65.0	65.0	65.0	65.0	65.0	65.0	65.0	65.0	65.0	65.0	51.6	50.7	50.6	50.5	50.4	50.4	50.4	50.3	50.3	50.2	50.2
0.07	63.5	63.5	63.5	63.6	63.6	63.6	63.6	63.6	63.6	63.6	63.6	63.7	50.3	49.3	49.2	49.1	48.9	49.0	48.9	48.8	48.8	48.7	48.7
0.13	62.1	62.1	62.1	62.1	62.2	62.2	62.2	62.2	62.3	62.3	62.3	62.3	49.1	47.8	47.7	47.6	47.3	47.4	47.3	47.3	47.2	47.1	47.1
0.20	60.6	60.7	60.7	60.8	60.8	60.8	60.9	60.9	60.9	61.0	61.0	61.0	47.8	46.3	46.1	46.0	45.7	45.8	45.7	45.6	45.5	45.4	45.4
0.27	59.3	59.3	59.4	59.4	59.5	59.5	59.5	59.6	59.6	59.7	59.7	59.7	46.5	44.7	44.5	44.3	44.0	44.1	44.0	43.9	43.8	43.7	43.6
0.33	57.8	57.9	57.9	58.0	58.0	58.1	58.1	58.2	58.2	58.3	58.3	58.3	45.4	43.1	42.9	42.6	42.2	42.4	42.2	42.2	42.0	41.9	41.8
0.40	56.4	56.5	56.5	56.6	56.6	56.7	56.7	56.8	56.9	56.9	56.9	57.0	44.2	41.4	41.2	40.9	40.4	40.5	40.4	40.3	40.1	40.0	39.9
0.47	55.0	55.1	55.1	55.2	55.3	55.3	55.4	55.4	55.5	55.6	55.6	55.6	43.1	39.7	39.3	39.0	38.4	38.6	38.4	38.3	38.0	37.9	37.8
0.53	53.7	53.7	53.8	53.9	53.9	54.0	54.0	54.1	54.2	54.2	54.3	54.3	41.9	37.8	37.4	36.9	36.3	36.5	36.2	36.1	35.8	35.6	35.5
0.60	52.2	52.2	52.3	52.5	52.6	52.6	52.7	52.8	52.8	52.9	52.9	53.0	36.3	35.8	35.3	34.8	34.0	34.2	33.9	33.8	33.4	33.2	33.0
0.67	50.6	50.7	50.8	51.0	51.1	51.2	51.3	51.4	51.4	51.5	51.6	51.6	33.9	33.4	33.0	32.5	31.5	31.8	31.5	31.4	30.8	30.6	30.4
0.73	49.1	49.2	49.4	49.6	49.8	49.8	49.9	50.1	50.2	50.3	50.3	50.4	31.1	30.7	30.2	29.8	29.4	29.2	28.8	28.7	28.1	27.8	27.6
0.80	47.5	47.7	47.9	48.2	48.3	48.4	48.6	48.7	48.9	49.0	49.1	49.2	27.9	27.5	27.1	26.7	26.4	26.2	25.9	25.5	25.2	25.0	24.6
0.87	45.6	45.9	46.2	46.5	46.8	46.9	47.1	47.3	47.5	47.7	47.8	47.9	24.2	23.8	23.5	23.2	23.0	22.8	22.6	22.3	22.1	21.9	21.7
0.93	43.7	44.1	44.4	44.8	45.1	45.3	45.6	45.9	46.1	46.4	46.5	46.6	19.9	19.7	19.5	19.3	19.2	19.1	19.0	18.8	18.7	18.5	18.4
1.00	41.6	42.1	42.5	43.0	43.4	43.5	43.9	44.3	44.6	44.9	45.0	45.2	15.0	15.0	15.0	15.0	15.0	15.0	15.0	15.0	15.0	15.0	15.0
	GAS OUTLET												AIR INLET									

Figure 11.- Flue gas and air temperature profiles for convection-condensation heat transfer with water evaporation into ambient air (ºC)

x/L	GAS INLET												AIR OUTLET											
0.07	0	0	0	0	0	0	0	0	0	0	0	0	0	0	0	0	0	0	0	0	0	0	0	0
0.13	0	0	0	0	0	0	0	0	0	0	0	0	0	0	0	0	0	0	0	0	0	0	0	0
0.20	0	0	0	0	0	0	0	0	0	0	0	0	0	0	0	0	0	0	0	0	0	0	0	0
0.27	0	0	0	0	0	0	0	0	0	0	0	0	0	0	0	0	0	0	0	0	0	0	0	0
0.33	0	0	0	0	0	0	0	0	0	0	0	0	0	0	0	0	0	0	0	0	0	0	0	0
0.40	0	0	0	0	0	0	0	0	0	0	0	0	0	0	0	0	0	0	0	0	0	0	0	0
0.47	0	0	0	0	0	0	0	0	0	0	0	0	0	0	0	0	0	0	0	0	0	0	0	0
0.53	0	0	0	0	0	0	0	0	0	0	0	0	0	0	0	0	0	0	0	0	0	0	0	0
0.60	0.4	0.4	0.2	0.1	0	0	0	0	0	0	0	0	-0.7	0	0	0	0	0	0	0	0	0	0	0
0.67	2.9	2.7	2.4	2.1	1.8	1.5	1.2	1.0	0.8	0.6	0.5	0.4	-4.9	-4.9	-4.8	-3.1	0	0	0	0	0	0	0	0
0.73	3.7	3.5	3.2	2.9	2.6	2.3	2.0	1.8	1.5	1.3	1.2	1.1	-5.7	-5.6	-5.5	-5.4	-5.3	-5.8	0	0	0	0	0	0
0.80	5.3	5.1	4.7	4.4	4.0	3.7	3.4	3.1	2.8	2.5	2.4	2.3	-6.3	-6.2	-6.1	-5.9	-5.7	-5.6	-5.5	-5.3	0	0	0	0
0.87	7.1	6.9	6.6	6.2	5.8	5.4	5.1	4.7	4.4	4.0	3.9	3.7	-6.9	-6.8	-6.5	-6.3	-6.1	-6.0	-5.8	-5.6	-5.4	-5.3	-6.1	0
0.93	7.5	7.4	7.1	6.9	6.6	6.2	5.9	5.6	5.3	5.0	4.8	4.7	-7.8	-7.6	-7.3	-7.0	-6.7	-6.5	-6.3	-6.0	-5.8	-5.6	-5.4	-5.3
1.00	8.2	8.1	7.9	7.7	7.5	7.3	7.0	6.7	6.4	6.2	6.0	5.9	-8.8	-8.6	-8.2	-7.7	-7.4	-7.2	-6.9	-6.5	-6.3	-6.0	-5.7	-5.6
	GAS OUTLET												AIR INLET											

Figure 12.- Condensed/Evaporated (-ve) water flow rate (mol/s) for convection-condensation heat transfer with water evaporation into ambient air

x/L	GAS INLET												AIR OUTLET										
0.00	65.0	65.0	65.0	65.0	65.0	65.0	65.0	65.0	65.0	65.0	65.0	65.0	52.0	51.9	51.9	51.8	51.8	51.7	51.7	51.6	51.6	51.5	51.5
0.07	63.6	63.7	63.7	63.7	63.7	63.7	63.7	63.7	63.8	63.8	63.8	63.8	50.6	50.5	50.5	50.4	50.3	50.3	50.3	50.2	50.1	50.1	50.0
0.13	62.3	62.3	62.3	62.4	62.4	62.4	62.4	62.5	62.5	62.5	62.5	62.5	49.1	49.1	49.0	48.9	48.9	48.9	48.8	48.7	48.7	48.6	48.6
0.20	60.9	61.0	61.0	61.1	61.1	61.1	61.2	61.2	61.2	61.3	61.3	61.3	47.6	47.6	47.5	47.4	47.4	47.4	47.3	47.2	47.2	47.1	47.1
0.27	59.6	59.7	59.7	59.8	59.8	59.8	59.9	59.9	60.0	60.0	60.0	60.0	46.1	46.0	45.9	45.9	45.8	45.8	45.7	45.7	45.6	45.5	45.5
0.33	58.2	58.3	58.3	58.4	58.4	58.5	58.5	58.6	58.6	58.7	58.7	58.7	44.5	44.4	44.4	44.3	44.3	44.2	44.2	44.1	44.0	44.0	43.9
0.40	56.9	56.9	57.0	57.0	57.1	57.1	57.2	57.2	57.3	57.4	57.4	57.4	42.9	42.8	42.8	42.7	42.6	42.6	42.5	42.5	42.4	42.3	42.3
0.47	55.5	55.6	55.6	55.7	55.7	55.8	55.8	55.9	56.0	56.0	56.1	56.1	41.2	41.2	41.1	41.0	40.9	40.9	40.8	40.8	40.7	40.6	40.5
0.53	54.1	54.2	54.2	54.3	54.4	54.4	54.5	54.6	54.6	54.7	54.7	54.8	39.5	39.4	39.3	39.2	39.2	39.1	39.1	39.0	38.9	38.8	38.8
0.60	52.7	52.8	52.9	52.9	53.0	53.1	53.1	53.2	53.3	53.3	53.4	53.4	37.6	37.5	37.5	37.4	37.3	37.3	37.2	37.1	37.0	37.0	36.9
0.67	51.3	51.4	51.5	51.6	51.7	51.7	51.9	52.0	52.0	52.1	52.2	52.2	35.5	35.4	35.3	35.2	35.1	35.1	35.0	34.9	34.9	34.8	34.7
0.73	50.1	50.2	50.3	50.4	50.5	50.5	50.7	50.8	50.9	51.0	51.1	51.1	32.8	32.8	32.7	32.6	32.5	32.5	32.4	32.3	32.2	32.2	32.1
0.80	49.0	49.1	49.3	49.4	49.5	49.5	49.7	49.8	49.9	49.9	50.1	50.1	29.7	29.6	29.5	29.4	29.4	29.3	29.2	29.2	29.1	29.0	29.0
0.87	48.0	48.2	48.3	48.4	48.5	48.6	48.8	48.9	49.0	49.1	49.2	49.2	25.8	25.7	25.6	25.6	25.5	25.5	25.4	25.4	25.3	25.2	25.2
0.93	47.2	47.3	47.5	47.6	47.7	47.8	48.0	48.1	48.2	48.3	48.4	48.4	20.9	20.9	20.9	20.8	20.8	20.8	20.7	20.7	20.7	20.6	20.6
1.00	46.3	46.4	46.6	46.8	46.9	47.0	47.2	47.3	47.4	47.6	47.6	47.7	15.0	15.0	15.0	15.0	15.0	15.0	15.0	15.0	15.0	15.0	15.0
	GAS OUTLET												AIR INLET										

Figure 13.- Flue gas and air temperature profiles (ºC) for convection-condensation heat transfer with 100% condensed water drainage.

x/L	GAS INLET												AIR OUTLET											
0.07	0	0	0	0	0	0	0	0	0	0	0	0	0	0	0	0	0	0	0	0	0	0	0	0
0.13	0	0	0	0	0	0	0	0	0	0	0	0	0	0	0	0	0	0	0	0	0	0	0	0
0.20	0	0	0	0	0	0	0	0	0	0	0	0	0	0	0	0	0	0	0	0	0	0	0	0
0.27	0	0	0	0	0	0	0	0	0	0	0	0	0	0	0	0	0	0	0	0	0	0	0	0
0.33	0	0	0	0	0	0	0	0	0	0	0	0	0	0	0	0	0	0	0	0	0	0	0	0
0.40	0	0	0	0	0	0	0	0	0	0	0	0	0	0	0	0	0	0	0	0	0	0	0	0
0.47	0	0	0	0	0	0	0	0	0	0	0	0	0	0	0	0	0	0	0	0	0	0	0	0
0.53	0	0	0	0	0	0	0	0	0	0	0	0	0	0	0	0	0	0	0	0	0	0	0	0
0.60	0	0	0	0	0	0	0	0	0	0	0	0	0	0	0	0	0	0	0	0	0	0	0	0
0.67	0.7	0.7	0.5	0.3	0.2	0.0	0	0	0	0	0	0	0	0	0	0	0	0	0	0	0	0	0	0
0.73	1.2	1.2	1.0	0.8	0.7	0.5	0.4	0.3	0.1	0.0	0	0	0	0	0	0	0	0	0	0	0	0	0	0
0.80	2.0	1.9	1.7	1.5	1.3	1.2	1.0	0.8	0.7	0.6	0.5	0.4	0	0	0	0	0	0	0	0	0	0	0	0
0.87	2.2	2.1	1.9	1.8	1.6	1.5	1.3	1.2	1.1	0.9	0.9	0.8	0	0	0	0	0	0	0	0	0	0	0	0
0.93	2.3	2.3	2.1	2.0	1.9	1.8	1.6	1.5	1.4	1.2	1.2	1.1	0	0	0	0	0	0	0	0	0	0	0	0
1.00	3.0	2.9	2.8	2.6	2.5	2.3	2.2	2.0	1.9	1.7	1.7	1.6	0	0	0	0	0	0	0	0	0	0	0	0
	GAS OUTLET												AIR INLET											

Figure 14.- Condensed water flow rate (mol/s) for convection-condensation heat transfer with 100% condensed water drainage.

5. Conclusions

Decarbonisation of electricity generation with thermal power plants equipped with post-combustion carbon capture in water constrained environments is only possible if dry cooling systems are in place. Dry cooling configurations, which consist of rotary heat exchangers using ambient air as the cooling fluid, can eliminate the water usage for cooling the flue gas upstream of the capture plant. This constitutes up to 30% of the total cooling water used in the steam cycle condenser of a ca. 800 MW_e natural gas combined cycle power plant.

Post-combustion carbon capture systems based on chemical absorption require that the flue gas temperature is adjusted to a specific solvent. A flue gas temperature as low as 35 ºC is possible at the outlet of an air/gas rotary heat exchanger by selecting appropriate heat transfer area and cooling air flow rate. Dry cooling systems can therefore be used with a wide range of solvents avoiding lock-in to a specific solvent technology. This work is particularly focused on low temperature applications below the flue gases dew point, since rotary heat exchangers are conventionally designed for non-saturation conditions in coal-fired power plants.

A sensitivity analysis shows that the contribution of the latent heat (44%) to the total heat transfer rate is approximately the same as the contribution of the sensible heat (56%) when the flue gas from an air-based combustion combined cycle gas turbine (CCGT) plants is cooled down to 35 ºC. It becomes more significant in a CCGT plant with exhaust gas recirculation at higher recirculation ratios, e.g. the latent heat contribution is 55% for 35% recirculation ratio. Thus, water condensation from the flue gas and subsequent evaporation into the ambient air stream enhances the overall heat transfer rate, yet process modelling shows that the convection-condensation heat transfer coefficient is up to six times higher than those for convection only. Moreover, the heat transfer is controlled by the water diffusion through the non-condensable gas boundary layer, and the resistance to heat transfer through the condensed phase can be neglected for the typical range of water concentration in the flue gas of a CCGT plant of 8 to 12 vol%. The form of condensation, i.e. film wise or drop wise condensation, does not have a significant effect for the modelling of the heat transfer.

In order to maintain the cooling capacity of an air/gas rotary heat exchanger, initially designed for no-condensation conditions, for operation below saturation temperatures, the condensate should remain on the surface of the metal elements and completely evaporate into the ambient air stream. For a CCGT plant with 35% exhaust gas recirculation ratio, it is possible to cool down the flue gases to ca. 43 ºC if the condensed water is completely evaporated into the air. Yet, if the condensed water completely drains off the rotary heat exchanger, the flue gas outlet temperature is ca. 47 ºC, considering an air/gas rotary heat exchanger size of 1 m length and 13 m diameter (inside the casing), and a cooling air flow rate of 350 kg/s in both cases.

For low temperature applications of rotary heat exchangers, it is necessary to select adequate operation conditions that prevent the carry-over of water droplets as condensation occurs, e.g. low flue gas velocity and upwards direction, and select adequate materials with high wettability, i.e. high free surface energy, and an adequate geometry of the specially formed metal elements. The model also predicts where water condensation occurs, so that enamelled heating elements are applied on the cold-end tiers to mitigate any possible long-term corrosion problems.

Acknowledgements

This research was carried out with financial support from the Engineering and Physical Science Research Council (Impact Acceleration Award EPSRC PII033) and Howden Group (Glasgow, Scotland) and Royal Academy of Engineering Research Fellowship (Dr. Mathieu Lucquiaud).

References

[1] Herraiz L, Hogg D, Cooper J, Gibbins J, Lucquiaud M. Reducing water usage with rotary regenerative gas / gas heat exchangers in natural gas- fi red power plants with post-combustion carbon capture. Energy 2015;90:1994–2005. doi:10.1016/j.energy.2015.07.032.

[2] IEA. Water for Energy: Is energy becoming a thirstier resource? World Energy Outlook 2012 2012:1–33. doi:10.1787/weo-2012-en.

[3] Byers EA, Hall JW, Amezaga JM. Electricity generation and cooling water use: UK pathways to 2050 2014;25:16–30.

[4] Environmental Agency (EA). Estimated abstractions from all surface and groundwaters by purpose and source: 2000 to 2016 2017.

[5] IEAGHG. Evaluation and Analysis of Water Usage of Power Plants with CO2 Capture. Report : 2010/05 March 2011.

[6] Cormos CC, Vatopoulos K, Tzimas E. Assessment of the consumption of water and construction materials in state-of-the-art fossil fuel power generation technologies involving CO2 capture. Energy 2013;51:37–49. doi:10.1016/j.energy.2012.12.050.

[7] Byers EA, Qadrdan M, Leathard A, Alderson D, Hall JW, Amezaga JM, et al. Cooling water for Britain's future electricity supply. Proc Inst Civ Eng - Energy 2015;168:188–204. doi:10.1680/ener.14.00028.

[8] Schakel W, Pfister S, Ramírez A. International Journal of Greenhouse Gas Control Exploring the potential impact of implementing carbon capture technologies in fossil fuel power plants on regional European water stress index levels. Int J Greenh Gas Control 2015;39:318–28. doi:10.1016/j.ijggc.2015.05.031.

[9] Zhai H, Rubin ES. Performance and cost of wet and dry cooling systems for pulverized coal power plants with and without carbon capture and storage. Energy Policy 2010;38:5653–60. doi:10.1016/j.enpol.2010.05.013.

[10] Zhai H, Rubin ES, Versteeg PL. Water use at pulverized coal power plants with postcombustion carbon capture and storage. Environ Sci Technol 2011;45:2479–85. doi:10.1021/es1034443.

[11] Macknick J, Sattler S, Averyt K, Clemmer S, Rogers J. The water implications of generating electricity: Water use across the United States based on different electricity pathways through 2050. Environ Res Lett 2012;7. doi:10.1088/1748-9326/7/4/045803.

[12] Pan L, Liu P, Ma L, Li Z. A supply chain based assessment of water issues in the coal industry in China. Energy Policy 2012;48:93–102. doi:10.1016/j.enpol.2012.03.063.

[13] Hadian S, Madani K. The water demand of energy: Implications for sustainable energy policy development. Sustain 2013;5:4674–87. doi:10.3390/su5114674.

[14] Kitto JB, Stultz SC. Steam, its generation and use. 41st Ed. The Babcock and Wilcox Company; 1992.

[15] ElKady AM, Evulet A, Brand A, Ursin TP, Lynghjem A. Application of Exhaust Gas Recirculation in a DLN F-Class Combustion System for Postcombustion Carbon Capture. J Eng Gas Turbines Power 2009;131:034505. doi:10.1115/1.2982158.

[16] Li H, Haugen G, Ditaranto M, Berstad D, Jordal K. Impacts of exhaust gas recirculation (EGR) on the natural gas combined cycle integrated with chemical absorption CO2 capture technology. Energy Procedia 2011;4:1411–8. doi:10.1016/j.egypro.2011.02.006.

[17] Herraiz L, Sánchez Fernández E, Palfi E, Lucquiaud M. Selective exhaust gas recirculation in combined cycle gas turbine power plants with post-combustion CO2 capture. Int J Greenh Gas Control 2018;71:303–21. doi:10.1016/j.ijggc.2018.01.017.

[18] Sanchez Fernandez E, Goetheer EL V, Manzolini G, Macchi E, Rezvani S, Vlugt TJH. Thermodynamic assessment of amine based CO2 capture technologies in power plants based on European Benchmarking Task Force methodology. Fuel 2014;129:318–29.

doi:10.1016/j.fuel.2014.03.042.
[19] Klein H, Eigenberger G. Approximate solutions for metallic regenerative heat exchangers. Int J Heat Mass Transf 2001;44:3553–63. doi:10.1016/S0017-9310(01)00010-2.
[20] Sadrameli SM. Mathematical models for the simulation of thermal regenerators: A state-of-the-art review. Renew Sustain Energy Rev 2016;58:462–76. doi:10.1016/j.rser.2015.12.154.
[21] Nair S, Verma S, Dhingra SC. Rotary heat exchanger performance with axial heat dispersion. Int J Heat Mass Transf 1998;41:2857–64. doi:10.1016/S0017-9310(98)00004-0.
[22] VDI Gesellschaft. VDI Heat Atlas. Second Edi. Springer-Verlag Berlin Heidelberg; 2010.
[23] Incropera FP, DeWitt DP, Bergman TL, Lavine AS. Fundamentals of Heat and Mass Transfer. Sixth Edit. Jonh Wiley & Sons; 2011.
[24] Zhai C, Archer DH, Fischer JC. Performance modeling of desiccant wheels (1): model development. Proc Energy Sustinablity 2008 2008;ES2008-541:1–11.
[25] Al-Ghamdi AS. Analysis of air-to-air rotary energy wheels. 2006.
[26] Chantana C, Kumar S. Experimental and theoretical investigation of air-steam condensation in a vertical tube at low inlet steam fractions. Appl Therm Eng 2013;54:399–412. doi:10.1016/j.applthermaleng.2013.02.024.
[27] Shi X, Che D, Agnew B, Gao J. An investigation of the performance of compact heat exchanger for latent heat recovery from exhaust flue gases. Int J Heat Mass Transf 2011;54:606–15. doi:10.1016/j.ijheatmasstransfer.2010.09.009.
[28] Huang J, Zhang J, Wang L. Review of vapor condensation heat and mass transfer in the presence of non-condensable gas. Appl Therm Eng 2015;89:469–84. doi:10.1016/j.applthermaleng.2015.06.040.
[29] Liang Y, Che D, Kang Y. Effect of vapor condensation on forced convection heat transfer of moistened gas. Heat Mass Transf 2007;43:677–86. doi:10.1007/s00231-006-0148-0.
[30] Che D, Da Y, Zhuang Z. Heat and mass transfer characteristics of simulated high moisture flue gases. Heat Mass Transf Und Stoffuebertragung 2005;41:250–6. doi:10.1007/s00231-004-0505-9.
[31] PSE. gPROMS ModelBuilder V4.1.0 / Windows 2018. http://www.psenterprise.com/modelbuilder.html (accessed January 1, 2018).
[32] Howden Group. OEM of regenerative rotary gas/gas heat exchangers 2018;Glasgow, U.
[33] Osakabe M, Ishida K, Yagi K, Itoh T, Ohmasa K. Condensation Heat Transfer on Tubes in Actual Flue Gas. Heat Transf - Asian Res 2001;30:139–51.
[34] Osakabe M, Horiki S, Hanaki Y. Prediction and Performance of Compact Heat Exchanger with Small Diameter Tubes for Latent Heat Recovery. J Environ Eng 2009;4:253–9. doi:10.1299/jee.4.36.

Nomenclature

A	Heat transfer area (m^2)
Cp	Specific heat at constant pressure (J kg^{-1} K^{-1})
$C_{p\,G}$	Specific heat of the gas at constant pressure (J kg^{-1} K^{-1})
$C_{p\,S}$	Specific heat of the solid at constant pressure (J kg^{-1} K^{-1})
$D_{hydraulic}$	Hydraulic diameter (m)
D_{ab}	Binary mass diffusivity (m^2 s^{-1})
f	Friction factor
$\dot{G}$	Gas molar flow rate per time section (mol/s)
h_{cv}	Convective heat transfer coefficient (W m^{-2} K^{-1})
h_{cd}	Conduction heat transfer coefficient (W m^{-2} K^{-1})
h_m	Convective mass transfer coefficient (kg $m^{-2}s^{-1}$), $h_m = h'_m \cdot \rho_{gas}$
$h_m{}'$	Convective mass transfer coefficient (m s^{-1})
$h_{overall}$	Overall heat transfer coefficient (W m^{-2} K^{-1})
H_{fg}	Specific latent heat of condensation (kJ kg^{-1})
j_D	Colburn j factor for mass transfer
j_H	Colburn j factor for heat transfer
k_L	Heat conductivity of the liquid film (W m^{-1} K^{-1})
L	Length of the wheel in axial direction (m)
Le	Lewis number
$\dot{m}$	Mass flow rate (kg s^{-1})
$\dot{m}_G$	Gas mass flow rate (kg/s)
m_S	Mass of the solid elements (kg)
mf	Mass fraction
MW	Molecular Weight (g mol^{-1})
$\dot{n}$	Molar flow rate (kg s^{-1})
n_G	Gas molar flow rate (kg/s)
Nu	Nusselt number
N_L	Number of sections in longitudinal direction/ tier steps (--)
N_τ	Number of time sectors or sectors in the angular direction (--)
P	Pressure (bar)
Pr	Prandtl number
Re	Reynolds number
$\dot{S}$	Solid supply rate per tier (kg/s)

Sh	Sherwood number
Sc	Schmidt number
St	Stanton number
T	Temperature (K, ºC)
T_G	Temperature of the gas (K)
T_S	Temperature of the solid (K)
$\dot{Q}$	Heat flow rate or heat transferred (W)
q	Heat flux (J s^{-1} m^{-2})
u	Gas velocity (m s^{-1})
y	Molar fraction

Greek symbols

μ	Viscosity (Pa s)
ρ	Density (kg m^{-3})
γ_{L-G}	Surface tension liquid-gas/vapour phase (J/m^2)
γ_{S-G}	Surface energy or interfacial energy between solid and gas/vapour phase (J/m^2)
γ_{S-L}	Surface energy or interfacial energy between solid and liquid phase (J/m^2)
δ_L	Condensed film thickness (m)
ω	Angular speed (rpm)

Subscripts

b	Bulk
cd	Condensation
cv	Convection
cf	Condensate film
eff	Effective
G	Gas
i	Interface
in	Inlet
j	stage in longitudinal/axial direction
out	Outlet
S	Solid
s	stage in angular direction
sat	Saturation

Appendix A. Reference natural gas combined cycle power plant

The reference plant is an 800 MWe air-fired NGCC (natural gas combined cycle) plant with a 2-on-1 configuration: two GE9371FB gas turbines with the flue gas exiting into two HRSGs, which jointly supply steam to a subcritical triple pressure steam cycle. The gas turbine operates at a TIT (turbine inlet temperature) of 1371 ºC and AFR (air fuel ratio) of 40.5 on mass basis, at ISO atmospheric conditions and 100% load, with a power output at coupling of 285 MWe. In a combined cycle, the remaining heat contained in the exhaust flue gas is partially recovered to generate steam at three pressure levels. Two post-combustion capture units with primary amine base solvent technology are implemented at the tail-end, one per each gas turbine – HRSG train. In each train, flue gas is cooled down before entering the absorber. The gas composition at the outlet is then calculated assuming a removal ratio of CO_2 of 90% and that gas leaves the water wash section saturated at a temperature of 45 ºC. Stream variables are shown in Table A.1.

Table A.1 Exhaust flue gas stream information at the HRSG at different recirculation ratios (per GT-HRSG-absorber train)

EGR ratio		**0**	**10**	**20**	**30**	**35**	**40**
Pressure (HRSG outlet)	Pa	101300	101300	101300	101300	101300	101300
Pressure (HRSG outlet)	bar	1.013	1.013	1.013	1.013	1.013	1.013
Temperature	K	390	389	389	388	388	388
Temperature	ºC	116.8	116.3	115.7	115.1	114.8	114.5
Dew temperature (1.013 bar)	K	316.8	318.1	319.3	320.4	321.0	321.5
Dew temperature (1.013 bar)	ºC	43.69	44.96	46.15	47.29	47.84	48.39
Molar flow rate	mol/s	23178	22977	22783	22596	22505	22416
Mass flow rate	kg/s	658	652	646	641	638	636
Molar Mass	g/mol	28.37	28.35	28.34	28.35	28.36	28.38
Composition							
CO_2	%mol	4.21	4.69	5.29	6.07	6.55	7.12
H_2O	%mol	8.82	9.42	10.02	10.62	10.92	11.22
N_2	%mol	74.21	74.09	74.05	74.14	74.26	74.43
O_2	%mol	11.87	10.92	9.75	8.28	7.38	6.33
Ar	%mol	0.89	0.89	0.89	0.89	0.89	0.89

Appendix B. Mathematical model for convective heat transfer in a rotary gas/gas heat exchanger

The mathematical model for convection heat transfer in the rotary wheel consists of a system of partial differential equations describing the process of heat transfer by convection in the system. The amount of energy lost/gained by the fluid is equal to the amount of energy transferred across the non-condensable gas boundary layer, which is equal to the amount of energy gained/lost by the metal elements, as indicated in Equation (13) and Equation (14), where T_S is the metal elements temperature, T_G is the gas/air temperature, $\dot{n}_G$ is the gas/air molar/mass flow rate, m_S is the total mass of metal elements, $C_{p\,G}$ and $C_{p\,S}$ are the gas and solid heat capacity respectively, A_s is the total surface heating area of the metal elements and h_{cv} is the convective heat transfer coefficient.

B.1 <u>*Energy balance*</u>

A numerical solution discretises the system into $N_L x N_\tau$ stages, as illustrated in Figure 6b. The partial differential equations can be written as indicated in Equations from (15) to (18). The incremental step in the axial direction Δx and in the rotational direction $\Delta\tau$ are defined in Equation (19) and Equation (20) respectively, where L is the length of the wheel, ω is the rotor angular speed, N_L and N_τ are the number of stages in the longitudinal/axial direction and in the angular direction respectively. The gas/air flow rate $(\dot{G})$ and the amount of solid moving $(\dot{S})$ in each stage are defined by Equation (21) and Equation (22) respectively.

$$\dot{n}_G \cdot C_{p\,G} \cdot \left(\frac{\partial T_G}{\partial x}\right) = h_{cv}\frac{A_s}{L}(T_S - T_G) \tag{13}$$

$$m_S \cdot C_{p\,S} \cdot \frac{1}{L} \cdot \left(\frac{\partial T_S}{\partial \tau}\right) = h_{cv}\frac{A_s}{L}(T_G - T_S) \tag{14}$$

$$\frac{\dot{G}_{(j-1,s)} \cdot C_{p\,G_{(j-1,s)}} \cdot T_{G_{(j-1,s)}} - \dot{G}_{(j,s)} \cdot C_{p\,G_{(j,s)}} \cdot T_{G_{(j,s)}}}{L/N_L} \cdot N_\tau = h_{cv_{(j,s)}}\frac{A_s}{L}\left(T_{G_{(j,s)}} - T_{S_{(j,s)}}\right) \tag{15}$$

$$\frac{\dot{S}_{(j,s-1)} \cdot C_{p\,S} \cdot T_{S_{(j,s-1)}} - \dot{S}_{(j,s)} \cdot C_{p\,S} \cdot T_{S_{(j,s)}}}{(60/\omega \cdot 1/2)/N_\tau} \cdot 60/\omega \cdot 1/2 \cdot N_L = h_{cv_{(j,s)}}\frac{A_s}{L}\left(T_{S_{(j,s)}} - T_{G_{(j,s)}}\right) \tag{16}$$

$$\dot{G}_{(j-1,s)} \cdot C_{p\,G_{(j-1,s)}} \cdot T_{G_{(j-1,s)}} - \dot{G}_{(j,s)} \cdot C_{p\,G_{(j,s)}} \cdot T_{G_{(j,s)}} = h_{cv_{(j,s)}}\frac{A_s}{N_\tau \cdot N_L}\left(T_{G_{(j,s)}} - T_{S_{(j,s)}}\right) \tag{17}$$

$$\dot{S}_{(j,s-1)} \cdot C_{p\,S} \cdot T_{S_{(j,s-1)}} - \dot{S}_{(j,s)} \cdot C_{p\,S} \cdot T_{S_{(j,s)}} = h_{cv_{(j,s)}}\frac{A_s}{N_\tau \cdot N_L}\left(T_{S_{(j,s)}} - T_{G_{(j,s)}}\right) \tag{18}$$

$$\Delta x = \frac{L}{N_L} \tag{19}$$

$$\Delta \tau = \frac{60/\omega \cdot 1/2}{N_\tau} \tag{20}$$

$$\dot{G} = \frac{\dot{n}_G}{N_\tau} \tag{21}$$

$$\dot{S} = \frac{m_S}{60/\omega \cdot 1/2 \cdot N_L} \tag{22}$$

for $j = 1 \dots N_L$(no. of longitudinal sections), $s = 1 \dots N_\tau$(no. of time sections)

The Chilton-Colburn J-factor analogy is used to determine the convection heat transfer coefficient h_{cv} from the friction factor f, as shown in Equation (23) and Equation (24). The values of the coefficient α and the exponent β of the J-factor in Equation (25) have been experimentally determined by Howden and are taken from the results of thermal performance analysis conducted in previous work [1].

$$St = \frac{h_{cv}}{Cp_{gas} \cdot \rho_{gas} \cdot u_{gas}} \tag{23}$$

$$J_H = \frac{f}{2} = St \cdot Pr^{2/3} \tag{24}$$

$$J_H = \alpha \cdot Re^{\beta} \tag{25}$$

Appendix C. Mathematical model for convection-condensation heat transfer in a rotary gas/gas heat exchanger

The mathematical model for convection-condensation heat transfer in a rotary heat exchanger with a bisector configuration consists of a system of partial differential equations which describe the processes of the sensible and latent heat transfer, shown in Equations (26) and (27), and the mass transfer due to water condensation/ evaporation in the system, shown in Equation (31). The amount of energy lost/gained by the fluid is equal to the amount of energy transferred across the non-condensable gas boundary layer, which is equal to the amount of energy gained/lost by the metal element. The thermal resistance to heat transfer through the condensed liquid film is neglected and, thus, the overall heat transfer coefficient, $h_{overall}$, is calculated as the convection-condensation heat transfer coefficient.

C.1 *Energy balance*

The finite difference equations derived from the partial differential equations for heat transfer as implemented in gPROMS are shown in Equation (28) and Equation (29), where h'_{fg} is the latent heat of condensation. The overall heat transfer coefficient, $h_{overall}$, is evaluated as indicated in Equation (30). This correlation is theoretically derived in Appendix D. The coefficient *C* and the exponent *m* are evaluated to match the value of the convective heat transfer coefficient when there is not water condensation.

$$\dot{n}_G \cdot C_{p\,G} \cdot \left(\frac{\partial T_G}{\partial x}\right) + h'_{fg}\left(\frac{\partial \dot{n}_{H2O\ gas}}{\partial x}\right) = h_{overall}\ \frac{A_s}{L}(T_S - T_G) \tag{26}$$

$$\dot{m}_S \cdot C_{p\,S} \cdot \frac{1}{L} \cdot \left(\frac{\partial T_S}{\partial \tau}\right) = h_{overall}\ \frac{A_s}{L}(T_G - T_S) \tag{27}$$

$$\begin{aligned}\left(\dot{G}_{(j-1,s)} \cdot C_{p\,G_{(j-1,s)}} \cdot T_{G\,(j-1,s)} - \dot{G}_{(j,s)} \cdot C_{p\,G_{(j,s)}} \cdot T_{G\,(j,s)}\right) + h'_{fg}\left(T_{S_{(j,s)}}\right) \\ \cdot \dot{n}_{H2O\ condensed_{(j,s)}} = h_{overall_{(j,s)}} \frac{A_s}{N_\tau \cdot N_L}\left(T_{G_{(j,s)}} - T_{S_{(j,s)}}\right)\end{aligned} \tag{28}$$

$$\dot{S} \cdot C_{p\,S} \cdot \left(T_{S_{(j,s-1)}} - T_{S_{(j,s)}}\right) = h_{overall_{(j,s)}} \frac{A_s}{N_\tau \cdot N_L}\left(T_{S_{(j,s)}} - T_{G_{(j,s)}}\right) \tag{29}$$

$$\frac{h_{overall_{(j,s)}} \cdot D_{hydraulic}}{k_{gas}} = C \cdot {Re_{(j,s)}}^{m} \cdot {Pr_{(j,s)}}^{1/3} \cdot \left(1 + {Le_{(j,s)}}^{-2/3} \cdot B_{(j,s)} \cdot {Ja_{(j,s)}}^{-1}\right) \tag{30}$$

for $j = 1 \ldots N_L$(no. of longitudinal sections), $s = 1 \ldots N_\tau$(no. of time sections)

C.2 *Mass balance*

The finite difference equations derived from the partial differential equations for mass transfer as implemented in gPROMS are shown in Equations (32), (33) and (34), where $\dot{n}_{H2O\ condensed}$is the amount of water condensed/ evaporated in each stage, $\dot{n}_{H2O\ on\ Solid\ surface}$is the cumulative amount

of condensed water on the metal elements and $y_{H2O,G}$ is the molar fraction of water vapour in the gas bulk. The molar fraction of water vapour at the liquid-vapour interface, $y_{H2O,i}$, is evaluated as indicated in Equation (35), where $P_{sat,H2O}$ is the saturation pressure of water vapour in the gas at the metal/solid elements temperature, T_S, and P_G is the total pressure. Since thermal resistance through the condensed liquid is neglected, the temperature at the liquid-vapour interface is the same as the temperature of the metal elements. The mass transfer coefficient, h_m, is evaluated according to the Chilton and Colburn J-factor analogy for heat and mass transfer which is explained in Appendix C and shown in Equation (36).

$$\left(\frac{\partial \dot{n}_{H2O\ G}}{\partial x}\right) = \dot{n}_G \cdot \left(\frac{\partial y_{H2O,G}}{\partial x}\right) = h_m \frac{A_s}{L}\left(y_{H2O,G} - y_{H2O,i}\right) \tag{31}$$

$$\left(\dot{G}_{(j-1,s)} \cdot y_{H2O,G_{(j-1,s)}} - \dot{G}_{(x,\tau)} \cdot y_{H2O,i_{(x,\tau)}}\right) = \dot{n}_{H2O\ condensed_{(j,s)}} \tag{32}$$

$$\left(\dot{n}_{H2O\ on\ Solid\ surface_{(j,s)}} - \dot{n}_{H2O\ on\ Solid\ surface_{(j,s-1)}}\right) = \dot{n}_{H2O\ condensed_{(j,s)}} \tag{33}$$

$$\dot{n}_{H2O\ condensed_{(j,s)}} = h_{m_{(j,s)}} \cdot \frac{A_s}{N_\tau \cdot N_L} \cdot \left(y_{H2O,G_{(j,s)}} - y_{H2O,i_{(j,s)}}\right) \tag{34}$$

$$y_{H2O,i_{(j,s)}} = y^*_{H2O_{(j,s)}} = \frac{P_{sat,H2O}\left(T_{S_{(j,s)}}\right)}{P_{G_{(j,s)}}} \tag{35}$$

$$h_{m_{(j,s)}} = \frac{h_{cv_{(j,s)}}}{\rho_{gas_{(j,s)}} \cdot Cp_{gas_{(j,s)}} \cdot Le^{2/3}_{(j,s)}} \tag{36}$$

for $j = 1 \ldots N_L$(no. of longitudinal sections), $s = 1 \ldots N_\tau$(no. of time sections)

C.3 *Periodic equilibrium conditions*

As inlet conditions, mass flow rate, composition, temperature and pressure are defined for the flue gas at the top of the wheel (j = N_L, ∀s), and for the air at the bottom of the wheel (j = 0, ∀s) to account for a counter current flow arrangement, as indicated in Equations from (37) to (39). The cooling/heating cycle requires to define the temperature of the metal elements and the amount of condensed water remaining on the surface of the metal elements at the boundaries between the heating and the cooling sections, as indicated in Equations from (40) to (43).

It has been assumed that the total amount of condensed water from the flue gas remains on the surface of the elements and it is therefore transferred to the heating section. Liquid water does not drain off the wheel.

Flue gas side (cooling) Air side (heating)

$$\dot{m}_{\mathrm{G}_{(N_L,s)}} = \dot{m}_{\mathrm{Gas_{IN}}} \qquad \dot{m}_{\mathrm{G}_{(0,s)}} = \dot{m}_{\mathrm{Air_{IN}}} \tag{37}$$

$$y_{H2O\,(N_L,s)} = y_{H2O\,\mathrm{Gas_{IN}}} \qquad y_{H2O\,(0,s)} = y_{H2O\,\mathrm{Air_{IN}}} \tag{38}$$

$$T_{\mathrm{G}_{(N_L,s)}} = T_{\mathrm{Gas_{IN}}} \qquad T_{\mathrm{G}_{(0,s)}} = T_{\mathrm{Air_{IN}}} \tag{39}$$

for $s = 1 \ldots N_\tau$(no. of time sections)

$$\left[T_{\mathrm{S}_{(j,0)}}\right]_{\mathrm{Heating}} = \left[T_{\mathrm{S}_{(N_L-j,\mathrm{N}_\tau)}}\right]_{\mathrm{Cooling}} \tag{40}$$

$$\left[m_{H2O\ on\ Solid\ surface_{(j,0)}}\right]_{\mathrm{Heating}} = \left[m_{H2O on\ Solid\ surface_{(N_L-j,\mathrm{N}_\tau)}}\right]_{\mathrm{Cooling}} \tag{41}$$

$$\left[T_{\mathrm{S}_{(N_L-j,0)}}\right]_{\mathrm{Cooling}} = \left[T_{\mathrm{S}_{(j,\mathrm{N}_\tau)}}\right]_{\mathrm{Heating}} \tag{42}$$

$$\left[m_{H2O\ on\ Solid\ surface_{(N_L-j,0)}}\right]_{\mathrm{Cooling}} = \left[m_{H2O\ on\ Solid\ surface_{(j,\mathrm{N}_\tau)}}\right]_{\mathrm{Heating}} \tag{43}$$

for $\mathrm{j} = 1 \ldots \mathrm{N_L}$(no. longitudinal sections), $\mathrm{s} = 1 \ldots \mathrm{N}_\tau$(no. of time sections)

Appendix D. The normalised correlation of convection-condensation heat transfer coefficient

A dimensional analysis leads to Equation (44), which includes the major influential factors of the convective-condensation heat transfer coefficient, $h_{overall}$. A dimensional parameter group Ch, known as *condensation heat transfer factor* or *condensation factor,* can be obtained and it is defined in Equation (45), where $T_{sat(pv)}$ is the saturation temperature corresponding to the partial pressure of vapour in the bulk gas, $p_{H2O,gas}$, and T_S is the surface temperature. Che et al. [30] propose a normalized correlation of convection-condensation heat transfer coefficient shown in Equation (46), where *C*, *m* and *n* are constants to be determined experimentally [30,33]. The Prandtl number can be assumed constant and an exponent of 1/3 is assumed as in forced convention heat transfer.

$$h_{overall} = f\left(\mu_{gas}, k_{gas}, Cp_{gas}, \rho_{gas}, D, T_{gas} - T_S, T_{sat} - T_S\right) \tag{44}$$

$$Ch = \frac{T_{sat(pv)} - T_S}{T_{gas} - T_S} \tag{45}$$

$$Nu_{overall} = \boldsymbol{C} \cdot Re^{\boldsymbol{m}} \cdot Pr^{1/3} \cdot Ch^{\boldsymbol{n}} \tag{46}$$

The use of the condensation factor presents however a limitation, since *Ch* tends to zero when the vapour mass fraction is small. Therefore, the correlation would only be applicable to relatively high vapour fractions. In order to overcome this limitation, the theoretical analysis conducted by Liang et al. [29] leads to a dimensionless parameters group known as *augmentation factor*. The augmentation factor takes into account the effect of condensation of a relatively small amount of water vapour on convection heat transfer. A correlation is then derived to evaluate the combined convection-condensation heat transfer coefficient [27,29].

The augmentation factor results from the mass balance for the condensed water vapour and the non-condensable gases in the mixture at the interface. The vapour must diffuse through the non-condensable gas boundary layer to reach the liquid-vapour interface. A mass balance at the interface for each component leads to Equation (47) and Equation (48), where $m''_{H2O,cond}$ is the mass transfer rate of condensing water per unit area, $m''_{non\ cond}$ is the mass transfer rate of non-condensable gases per unit area, $mf_{H2O,i}$ is the water vapour mass fraction and $mf_{non\ cond,i}$ the mass fraction of non-condensable gases at the interface. Considering a mixture of only two components, condensing vapour and non-condensable gases and conditions in Equation (49) and (50), Equations (47) and Equation (48) can be combined to obtain Equation (51), where h_m is the mass transfer coefficient and *B* is the driving force for mass transfer.

$$m''_{H2O,cond} = m''_{total,\,i} \cdot mf_{H2O,i} + \left(-\rho D \frac{\partial mf_{H2O}}{\partial y}\right)_i \tag{47}$$

$$m''_{non\ cond} = m''_{total,\,i} \cdot mf_{non\ cond,i} + \left(-\rho D \frac{\partial mf_{non\ cond}}{\partial y}\right)_i = 0 \tag{48}$$

$$mf_{H2O} + mf_{non\ cond} = 1 \tag{49}$$

$$\frac{\partial mf_{H2O}}{\partial y} + \frac{\partial mf_{non\ cond}}{\partial y} = 0 \tag{50}$$

$$m''_{H2O,cond} = \frac{\left(-\rho D \frac{\partial mf_{H2O}}{\partial y}\right)_i}{1 - mf_{H2O,i}} = h_m \frac{\left(\boldsymbol{mf_{H2O,gas} - mf_{H2O,i}}\right)}{\left(\boldsymbol{1 - mf_{H2O,i}}\right)} = h_m \cdot \boldsymbol{B} \tag{51}$$

In the condensation process, the mass fraction of water vapour at the interface, $mf_{H2O,i}$, can be considered equal to the value corresponding to a saturated gas at the surface temperature if the resistance of the condensate film is neglected.

The condensation heat transfer coefficient h_{cond} can be defined as a function of the mass transfer rate of condensed water, as shown in Equation (53). This equation results from substituting Equation (51) into the expression for the latent heat transfer rate through the interface between the bulk gas and the gas boundary layer, Equation (52).

$$d\dot{Q}_{condensation} = H_{fg} \cdot m''_{H2O,cond} \cdot dA = h_{cond} \cdot \left(T_{gas} - T_i\right) \cdot dA \tag{52}$$

$$h_{cond} = \frac{H_{fg} \cdot m''_{H2O,cond}}{\left(T_{gas} - T_i\right)} = \frac{H_{fg} \cdot h_m \cdot B}{\left(T_{gas} - T_i\right)} \tag{53}$$

According to the definition of the Nusselt number, Equation (54) can be obtained. By using the definition of the Sherwood number (Sh), Equation (54) can be written as Equation (55), where Sc/Pr is the Lewis number (Le) and the group $Cp_{gas} \cdot \left(T_{gas} - T_i\right)/H_{fg}$ is the ratio of the sensible heat transfer to the heat of phase change, known as Jakob number (Ja).

$$Nu_{cond} = \frac{h_{cond} \cdot D_{hydraulic}}{k_{gas}} = \frac{H_{fg} \cdot h_m \cdot B}{\left(T_{gas} - T_i\right)} \cdot \frac{D_{hydraulic}}{k_{gas}} \tag{54}$$

$$Nu_{cond} = Sh \cdot B \cdot \frac{H_{fg}}{Cp_{gas} \cdot \left(T_{gas} - T_i\right)} \cdot \frac{Pr}{Sc} \tag{55}$$

$$Nu_{cond} = Sh \cdot B \cdot Ja^{-1} \cdot Le^{-1} \tag{56}$$

$$Nu_{cond} = C' \cdot Re^{m'} \cdot Pr^{1/3} \cdot Le^{-2/3} \cdot B \cdot Ja^{-1} \tag{57}$$

The Nusselt number for the overall heat transfer coefficient of both sensible and latent components is obtained combining Equation (57) and (58). Using the analogy for mass transfer and heat transfer, it can be assumed $C' = C$ and $m' = m$, leading to Equation (59).The mass transfer expression

described by the Sherwood number is identical to the heat transfer expression described by the Nusselt number for the same boundary conditions, as explained in Appendix A.

$$Nu_{cv} = C \cdot Re^{m} \cdot Pr^{1/3} \tag{58}$$

$$Nu_{overall} = Nu_{cond} + Nu_{cv} = C \cdot Re^{m} \cdot Pr^{1/3} \cdot \left(1 + Le^{-2/3} \cdot B \cdot Ja^{-1}\right) \tag{59}$$

$$augmentation\ factor \equiv \left(1 + Le^{-2/3} \cdot B \cdot Ja^{-1}\right) \tag{60}$$

Equation (59) is the normalized correlation of convection-condensation heat transfer, in which ***C*** and ***m*** are constant to be determined from experimental data. The augmentation factor, shown in Equation (60), therefore accounts for the enhancement effect induced by condensation of water vapour on forced convection heat transfer [29]. A qualitative analysis of Equation (59) shows that if the vapour mass fraction is zero, i.e. $mf_{H2O,gas} = mf_{H2O,i} = 0$, B will be equal to zero and the augmentation factor is reduced to unit. Consequently, Equation (59) is reduced to the form of the Nusselt number for convection heat transfer without condensation.

Equation (61) and Equation (62) indicate that the *condensation factor* and the *augmentation factor* have the same physical meaning.

$$1/Ja = \frac{H_{fg}}{Cp_{gas} \cdot \left(T_{gas} - T_{w}\right)} \approx \frac{1}{\left(T_{gas} - T_{w}\right)} \tag{61}$$

$$Ch = \frac{T_{sat(pv)} - T_{w}}{T_{gas} - T_{w}} \approx \frac{1}{\left(T_{gas} - T_{w}\right)} \tag{62}$$

Appendix E. Chilton and Colburn J-factor analogy

The Chilton and Colburn J-factor analogy establishes an analogy between heat, momentum and mass transfer. Equation (63) permits therefore the prediction of heat transfer coefficient, mass transfer coefficient or friction factor when one of the others is known. J_H is the J-factor for heat transfer, J_D is the J-factor for mass transfer and f is the friction factor, defined as indicated in Equations (64) and (66). The analogy is valid for fully developed turbulent flow when Re > 10,000 and for ranges 0.6 < Sc < 2500 and 0.6 < Pr < 100.

$$J_D = J_H = \frac{f}{2} \tag{63}$$

$$J_H = \frac{f}{2} = St \cdot Pr^{2/3} = \frac{h_{cv}}{\rho_{gas} \cdot Cp_{gas} \cdot v_{gas}} Pr^{2/3} \tag{64}$$

$$J_H = \alpha \cdot Re^{\beta} \tag{65}$$

$$J_D = St_m \cdot Sc^{2/3} = \frac{h_m}{v_{gas}} Sc^{2/3} \tag{66}$$

$$\frac{h_m}{h_{cv}} = \frac{1}{\rho_{gas} \cdot Cp_{gas} \cdot Le^{2/3}} \tag{67}$$

Force convection heat transfer and mass transfer can therefore be described by the Nusselt number (*Nu*) and the Sherwood number (*Sh*), as indicated in Equations (68) and (69). For a given process, if the boundary conditions are the same, there is an analogy between the heat transfer and the mass transfer. Thus the coefficients and the exponents in Equations (68) and (69) should be identical. Equation (71) relates mass transfer coefficient (h_m) and heat transfer coefficient (h_{cv}) and gives a good prediction when the steam mass concentrations was less than 25% [34].

$$Nu = C \cdot Re^{m} \cdot Pr^{1/3} \tag{68}$$

$$Sh = C' \cdot Re^{m'} \cdot Sc^{1/3} \tag{69}$$

$$\frac{Nu}{Sh} = \left(\frac{Pr}{Sc}\right)^{1/3} \tag{70}$$

$$\frac{h_{cv}}{h_m} = \rho_{gas} \cdot Cp_{gas} \cdot \left(\frac{Sc}{Pr}\right)^{2/3} = \rho_{gas} \cdot Cp_{gas} \cdot Le^{2/3} \tag{71}$$

Dimensionless numbers

Jacob number $$Ja = \frac{Cp_{gas} \cdot \left(T_{gas} - T_i\right)}{H_{fg}} \quad (72)$$

Lewis number $$Le = \frac{Sc}{Pr} \quad (73)$$

Nusselt number $$Nu = \frac{h \cdot D_{hydraulic}}{k_{gas}} \quad (74)$$

Prandtl number $$Pr = \frac{\mu_{gas} \cdot Cp_{gas}}{k_{gas}} \quad (75)$$

Reynolds number $$Re = \frac{\rho_{gas} \cdot u_{gas} \cdot D_{hydraulic}}{\mu_{gas}} \quad (76)$$

Stanton number $$St = \frac{h}{Cp_{gas} \cdot \rho_{gas} \cdot u_{gas}} \quad (77)$$

Sherwood number $$Sh = \frac{h_m \cdot D_{hydraulic}}{\rho_{gas} \cdot D_{ab}} \quad (78)$$

Schmidt number $$Sc = \frac{\mu_{gas}}{\rho_{gas} \cdot D_{ab}} \quad (79)$$

Appendix F. Variables profiles predicted from the gPROMS model of an air/gas rotary heat exchanger

F.1.- Convection-condensation heat transfer with water evaporation

Process modelling of a rotary air/gas heat exchanger for the flue gas cooling in a HRSG with EGR at 35% recirculation ratio is conducted first assuming that all the condensed water remains on the metal surface and it is completely evaporated into the ambient air stream. Results are discussed in Section 4.2.1 and presented here in terms of the flue gases temperature profile (Figure F.1), the metal temperature profile (Figure F.2), the water condensation (+ve) and evaporation (-ve) flow rate profile (Figure F.3) and the augmentation factor values at different locations in the rotary heat exchanger (Figure F.4).

x/L	GAS INLET												AIR OUTLET										
0.00	65.0	65.0	65.0	65.0	65.0	65.0	65.0	65.0	65.0	65.0	65.0	65.0	51.6	50.7	50.6	50.5	50.4	50.4	50.4	50.3	50.3	50.2	50.2
0.07	63.5	63.5	63.5	63.6	63.6	63.6	63.6	63.6	63.6	63.6	63.6	63.7	50.3	49.3	49.2	49.1	48.9	49.0	48.9	48.8	48.8	48.7	48.7
0.13	62.1	62.1	62.1	62.1	62.2	62.2	62.2	62.2	62.3	62.3	62.3	62.3	49.1	47.8	47.7	47.6	47.3	47.4	47.3	47.3	47.2	47.1	47.1
0.20	60.6	60.7	60.7	60.8	60.8	60.8	60.9	60.9	60.9	61.0	61.0	61.0	47.8	46.3	46.1	46.0	45.7	45.8	45.7	45.6	45.5	45.4	45.4
0.27	59.3	59.3	59.4	59.4	59.5	59.5	59.5	59.6	59.6	59.7	59.7	59.7	46.5	44.7	44.5	44.3	44.0	44.1	44.0	43.9	43.8	43.7	43.6
0.33	57.8	57.9	57.9	58.0	58.0	58.1	58.1	58.2	58.2	58.3	58.3	58.3	45.4	43.1	42.9	42.6	42.2	42.4	42.2	42.2	42.0	41.9	41.8
0.40	56.4	56.5	56.5	56.6	56.6	56.7	56.7	56.8	56.9	56.9	56.9	57.0	44.2	41.4	41.2	40.9	40.4	40.5	40.4	40.3	40.1	40.0	39.9
0.47	55.0	55.1	55.1	55.2	55.3	55.3	55.4	55.4	55.5	55.6	55.6	55.6	43.1	39.7	39.3	39.0	38.4	38.6	38.4	38.3	38.0	37.9	37.8
0.53	53.7	53.7	53.8	53.9	53.9	54.0	54.0	54.1	54.2	54.2	54.3	54.3	41.9	37.8	37.4	36.9	36.3	36.5	36.2	36.1	35.8	35.6	35.5
0.60	52.2	52.2	52.3	52.5	52.6	52.6	52.7	52.8	52.8	52.9	52.9	53.0	36.3	35.8	35.3	34.8	34.0	34.2	33.9	33.8	33.4	33.2	33.0
0.67	50.6	50.7	50.8	51.0	51.1	51.2	51.3	51.4	51.4	51.5	51.6	51.6	33.9	33.4	33.0	32.5	31.5	31.8	31.5	31.4	30.8	30.6	30.4
0.73	49.1	49.2	49.4	49.6	49.8	49.8	49.9	50.1	50.2	50.3	50.3	50.4	31.1	30.7	30.2	29.8	29.4	29.2	28.8	28.7	28.1	27.8	27.6
0.80	47.5	47.7	47.9	48.2	48.3	48.4	48.6	48.7	48.9	49.0	49.1	49.2	27.9	27.5	27.1	26.7	26.4	26.2	25.9	25.5	25.2	25.0	24.6
0.87	45.6	45.9	46.2	46.5	46.8	46.9	47.1	47.3	47.5	47.7	47.8	47.9	24.2	23.8	23.5	23.2	23.0	22.8	22.6	22.3	22.1	21.9	21.7
0.93	43.7	44.1	44.4	44.8	45.1	45.3	45.6	45.9	46.1	46.4	46.5	46.6	19.9	19.7	19.5	19.3	19.2	19.1	19.0	18.8	18.7	18.5	18.4
1.00	41.6	42.1	42.5	43.0	43.4	43.5	43.9	44.3	44.6	44.9	45.0	45.2	15.0	15.0	15.0	15.0	15.0	15.0	15.0	15.0	15.0	15.0	15.0
	GAS OUTLET												AIR INLET										

Figure F.1.- Flue gas and air temperature profiles for convection-condensation heat transfer with water evaporation into ambient air (ºC)

x/L	GAS INLET											AIR OUTLET										
0.07	55.5	55.6	55.7	55.8	55.9	56.0	56.1	56.2	56.3	56.4	56.5	57.4	57.3	57.3	57.2	57.2	57.1	57.1	57.0	57.0	56.9	56.9
0.13	54.4	54.5	54.6	54.7	54.8	54.9	55.0	55.1	55.1	55.2	55.3	56.1	56.1	56.0	56.0	55.9	55.9	55.8	55.8	55.7	55.7	55.6
0.20	53.3	53.4	53.5	53.6	53.7	53.7	53.8	53.9	54.0	54.1	54.2	54.9	54.9	54.8	54.8	54.7	54.6	54.6	54.5	54.5	54.4	54.4
0.27	52.2	52.3	52.4	52.5	52.6	52.6	52.7	52.8	52.9	53.0	53.1	53.7	53.6	53.6	53.5	53.5	53.4	53.3	53.3	53.2	53.2	53.1
0.33	50.3	50.4	50.5	50.6	50.7	50.8	50.9	51.0	51.0	51.1	51.2	52.0	51.9	51.9	51.8	51.7	51.7	51.6	51.6	51.5	51.4	51.4
0.40	49.2	49.3	49.4	49.5	49.6	49.7	49.7	49.8	49.9	50.0	50.1	50.7	50.7	50.6	50.6	50.5	50.4	50.4	50.3	50.2	50.2	50.1
0.47	48.1	48.2	48.3	48.4	48.5	48.5	48.6	48.7	48.8	48.9	49.0	49.5	49.4	49.4	49.3	49.2	49.2	49.1	49.0	49.0	48.9	48.8
0.53	47.0	47.1	47.2	47.3	47.4	47.4	47.5	47.6	47.7	47.8	47.9	48.2	48.2	48.1	48.0	48.0	47.9	47.8	47.7	47.7	47.6	47.5
0.60	45.9	46.0	46.1	46.2	46.3	46.4	46.5	46.5	46.6	46.7	46.8	46.9	46.7	46.7	46.6	46.5	46.4	46.4	46.3	46.2	46.1	46.0
0.67	43.9	44.2	44.5	44.7	45.0	45.2	45.4	45.5	45.7	45.8	46.0	46.0	45.6	45.1	44.6	44.6	44.5	44.4	44.3	44.2	44.1	44.1
0.73	42.7	43.1	43.4	43.8	44.1	44.3	44.6	44.8	45.0	45.2	45.4	45.3	44.8	44.2	43.7	43.2	42.8	42.8	42.7	42.6	42.5	42.4
0.80	40.6	41.1	41.6	42.0	42.4	42.8	43.2	43.5	43.8	44.1	44.3	44.2	43.5	42.9	42.4	41.8	41.2	40.7	40.1	40.0	40.0	39.8
0.87	37.6	38.2	38.9	39.5	40.1	40.6	41.1	41.6	42.0	42.4	42.8	42.5	41.9	41.2	40.6	39.9	39.3	38.8	38.2	37.7	37.1	36.8
0.93	35.4	36.1	36.8	37.4	38.1	38.7	39.2	39.8	40.3	40.8	41.3	40.9	40.1	39.4	38.6	38.0	37.3	36.7	36.1	35.5	34.9	34.4
1.00	32.4	33.2	33.9	34.7	35.4	36.1	36.8	37.4	38.0	38.6	39.2	38.8	37.9	37.1	36.3	35.5	34.8	34.1	33.5	32.9	32.3	31.7
	GAS OUTLET											AIR INLET										

Figure F.2.- Metal elements temperature profiles for convection-condensation heat transfer with water evaporation into ambient air (ºC)

x/L	GAS INLET												AIR OUTLET											
0.07	0	0	0	0	0	0	0	0	0	0	0	0	0	0	0	0	0	0	0	0	0	0	0	0
0.13	0	0	0	0	0	0	0	0	0	0	0	0	0	0	0	0	0	0	0	0	0	0	0	0
0.20	0	0	0	0	0	0	0	0	0	0	0	0	0	0	0	0	0	0	0	0	0	0	0	0
0.27	0	0	0	0	0	0	0	0	0	0	0	0	0	0	0	0	0	0	0	0	0	0	0	0
0.33	0	0	0	0	0	0	0	0	0	0	0	0	0	0	0	0	0	0	0	0	0	0	0	0
0.40	0	0	0	0	0	0	0	0	0	0	0	0	0	0	0	0	0	0	0	0	0	0	0	0
0.47	0	0	0	0	0	0	0	0	0	0	0	0	0	0	0	0	0	0	0	0	0	0	0	0
0.53	0	0	0	0	0	0	0	0	0	0	0	0	0	0	0	0	0	0	0	0	0	0	0	0
0.60	0.4	0.4	0.2	0.1	0	0	0	0	0	0	0	0	-0.7	0	0	0	0	0	0	0	0	0	0	0
0.67	2.9	2.7	2.4	2.1	1.8	1.5	1.2	1.0	0.8	0.6	0.5	0.4	-4.9	-4.9	-4.8	-3.1	0	0	0	0	0	0	0	0
0.73	3.7	3.5	3.2	2.9	2.6	2.3	2.0	1.8	1.5	1.3	1.2	1.1	-5.7	-5.6	-5.5	-5.4	-5.3	-5.8	0	0	0	0	0	0
0.80	5.3	5.1	4.7	4.4	4.0	3.7	3.4	3.1	2.8	2.5	2.4	2.3	-6.3	-6.2	-6.1	-5.9	-5.7	-5.6	-5.5	-5.3	0	0	0	0
0.87	7.1	6.9	6.6	6.2	5.8	5.4	5.1	4.7	4.4	4.0	3.9	3.7	-6.9	-6.8	-6.5	-6.3	-6.1	-6.0	-5.8	-5.6	-5.4	-5.3	-6.1	0
0.93	7.5	7.4	7.1	6.9	6.6	6.2	5.9	5.6	5.3	5.0	4.8	4.7	-7.8	-7.6	-7.3	-7.0	-6.7	-6.5	-6.3	-6.0	-5.8	-5.6	-5.4	-5.3
1.00	8.2	8.1	7.9	7.7	7.5	7.3	7.0	6.7	6.4	6.2	6.0	5.9	-8.8	-8.6	-8.2	-7.7	-7.4	-7.2	-6.9	-6.5	-6.3	-6.0	-5.7	-5.6
	GAS OUTLET												AIR INLET											

Figure F.3.- Condensed (+ve) /Evaporated (-ve) water flow rate (mol/s) for convection-condensation heat transfer with water evaporation into ambient air

x/L	GAS INLET												AIR OUTLET											
0.00	1.0	1.0	1.0	1.0	1.0	1.0	1.0	1.0	1.0	1.0	1.0	1.0	1.0	1.0	1.0	1.0	1.0	1.0	1.0	1.0	1.0	1.0	1.0	1.0
0.07	1.0	1.0	1.0	1.0	1.0	1.0	1.0	1.0	1.0	1.0	1.0	1.0	1.0	1.0	1.0	1.0	1.0	1.0	1.0	1.0	1.0	1.0	1.0	1.0
0.13	1.0	1.0	1.0	1.0	1.0	1.0	1.0	1.0	1.0	1.0	1.0	1.0	1.0	1.0	1.0	1.0	1.0	1.0	1.0	1.0	1.0	1.0	1.0	1.0
0.20	1.0	1.0	1.0	1.0	1.0	1.0	1.0	1.0	1.0	1.0	1.0	1.0	1.0	1.0	1.0	1.0	1.0	1.0	1.0	1.0	1.0	1.0	1.0	1.0
0.27	1.0	1.0	1.0	1.0	1.0	1.0	1.0	1.0	1.0	1.0	1.0	1.0	1.0	1.0	1.0	1.0	1.0	1.0	1.0	1.0	1.0	1.0	1.0	1.0
0.33	1.0	1.0	1.0	1.0	1.0	1.0	1.0	1.0	1.0	1.0	1.0	1.0	1.0	1.0	1.0	1.0	1.0	1.0	1.0	1.0	1.0	1.0	1.0	1.0
0.40	1.0	1.0	1.0	1.0	1.0	1.0	1.0	1.0	1.0	1.0	1.0	1.0	1.0	1.0	1.0	1.0	1.0	1.0	1.0	1.0	1.0	1.0	1.0	1.0
0.47	1.0	1.0	1.0	1.0	1.0	1.0	1.0	1.0	1.0	1.0	1.0	1.0	1.0	1.0	1.0	1.0	1.0	1.0	1.0	1.0	1.0	1.0	1.0	1.0
0.53	1.2	1.2	1.1	1.0	1.0	1.0	1.0	1.0	1.0	1.0	1.0	1.0	1.0	1.0	1.0	1.0	1.0	1.0	1.0	1.0	1.0	1.0	1.0	1.0
0.60	3.2	3.1	2.9	2.7	2.5	2.3	2.1	1.9	1.7	1.5	1.4	1.3	6.0	1.0	1.0	1.0	1.0	1.0	1.0	1.0	1.0	1.0	1.0	1.0
0.67	4.2	4.1	3.9	3.8	3.5	3.3	3.1	2.9	2.7	2.5	2.3	2.2	5.7	5.7	5.6	5.6	5.7	5.4	1.0	1.0	1.0	1.0	1.0	1.0
0.73	5.1	5.0	4.9	4.9	4.7	4.5	4.4	4.2	4.0	3.8	3.6	3.5	5.6	5.6	5.5	5.5	5.4	5.3	5.5	5.5	1.0	1.0	1.0	1.0
0.80	5.5	5.5	5.5	5.5	5.4	5.3	5.2	5.2	5.0	4.9	4.8	4.7	5.5	5.4	5.4	5.3	5.2	5.2	5.1	5.1	5.1	5.1	4.7	1.0
0.87	5.5	5.5	5.5	5.6	5.6	5.6	5.6	5.5	5.5	5.5	5.4	5.4	5.3	5.2	5.2	5.1	5.1	5.0	4.9	4.9	4.8	4.8	4.7	4.8
0.93	5.3	5.4	5.4	5.5	5.5	5.6	5.6	5.7	5.7	5.7	5.7	5.7	5.2	5.2	5.1	5.0	5.0	4.9	4.9	4.8	4.7	4.7	4.7	4.6
1.00	5.4	5.5	5.6	5.6	5.7	5.7	5.7	5.8	5.8	5.8	5.8	5.8	5.2	5.1	5.1	5.0	5.0	4.9	4.8	4.8	4.7	4.7	4.7	4.7
	GAS OUTLET												AIR INLET											

Figure F.4.- Augmentation factors for convection-condensation heat transfer with water evaporation into ambient air

F.2.- Convection-condensation heat transfer with water drainage

Process modelling of a rotary air/gas heat exchanger for the flue gas cooling in a HRSG with EGR at 35% recirculation ratio is conducted assuming that all the condensed completely drains off the system. Results are discussed in Section 4.2.2 and presented here in terms of the flue gases temperature profile (Figure F.5), the metal temperature profile (Figure F.6), the water condensation (+ve) and evaporation (-ve) flow rate profile (Figure F.7) and the augmentation factor values at different locations in the rotary heat exchanger (Figure F.8).

x/L	GAS INLET												AIR OUTLET										
0.00	65.0	65.0	65.0	65.0	65.0	65.0	65.0	65.0	65.0	65.0	65.0	65.0	52.0	51.9	51.9	51.8	51.8	51.7	51.7	51.6	51.6	51.5	51.5
0.07	63.6	63.7	63.7	63.7	63.7	63.7	63.7	63.7	63.8	63.8	63.8	63.8	50.6	50.5	50.5	50.4	50.3	50.3	50.3	50.2	50.1	50.1	50.0
0.13	62.3	62.3	62.3	62.4	62.4	62.4	62.4	62.5	62.5	62.5	62.5	62.5	49.1	49.1	49.0	48.9	48.9	48.9	48.8	48.7	48.7	48.6	48.6
0.20	60.9	61.0	61.0	61.1	61.1	61.1	61.2	61.2	61.2	61.3	61.3	61.3	47.6	47.6	47.5	47.4	47.4	47.4	47.3	47.2	47.2	47.1	47.1
0.27	59.6	59.7	59.7	59.8	59.8	59.8	59.9	59.9	60.0	60.0	60.0	60.0	46.1	46.0	45.9	45.9	45.8	45.8	45.7	45.7	45.6	45.5	45.5
0.33	58.2	58.3	58.3	58.4	58.4	58.5	58.5	58.6	58.6	58.7	58.7	58.7	44.5	44.4	44.4	44.3	44.3	44.2	44.2	44.1	44.0	44.0	43.9
0.40	56.9	56.9	57.0	57.0	57.1	57.1	57.2	57.2	57.3	57.4	57.4	57.4	42.9	42.8	42.8	42.7	42.6	42.6	42.5	42.5	42.4	42.3	42.3
0.47	55.5	55.6	55.6	55.7	55.7	55.8	55.8	55.9	56.0	56.0	56.1	56.1	41.2	41.2	41.1	41.0	40.9	40.9	40.8	40.8	40.7	40.6	40.5
0.53	54.1	54.2	54.2	54.3	54.4	54.4	54.5	54.6	54.6	54.7	54.7	54.8	39.5	39.4	39.3	39.2	39.2	39.1	39.1	39.0	38.9	38.8	38.8
0.60	52.7	52.8	52.9	52.9	53.0	53.1	53.1	53.2	53.3	53.3	53.4	53.4	37.6	37.5	37.5	37.4	37.3	37.3	37.2	37.1	37.0	37.0	36.9
0.67	51.3	51.4	51.5	51.6	51.7	51.7	51.9	52.0	52.0	52.1	52.2	52.2	35.5	35.4	35.3	35.2	35.1	35.1	35.0	34.9	34.9	34.8	34.7
0.73	50.1	50.2	50.3	50.4	50.5	50.5	50.7	50.8	50.9	51.0	51.1	51.1	32.8	32.8	32.7	32.6	32.5	32.5	32.4	32.3	32.2	32.2	32.1
0.80	49.0	49.1	49.3	49.4	49.5	49.5	49.7	49.8	49.9	49.9	50.1	50.1	29.7	29.6	29.5	29.4	29.4	29.3	29.2	29.2	29.1	29.0	29.0
0.87	48.0	48.2	48.3	48.4	48.5	48.6	48.8	48.9	49.0	49.1	49.2	49.2	25.8	25.7	25.6	25.6	25.5	25.5	25.4	25.4	25.3	25.2	25.2
0.93	47.2	47.3	47.5	47.6	47.7	47.8	48.0	48.1	48.2	48.3	48.4	48.4	20.9	20.9	20.9	20.8	20.8	20.8	20.7	20.7	20.7	20.6	20.6
1.00	46.3	46.4	46.6	46.8	46.9	47.0	47.2	47.3	47.4	47.6	47.6	47.7	15.0	15.0	15.0	15.0	15.0	15.0	15.0	15.0	15.0	15.0	15.0
	GAS OUTLET												AIR INLET										

Figure F.5.- Flue gas and air temperature profiles (ºC) for convection-condensation heat transfer with 100% condensed water drainage.

x/L	GAS INLET											AIR OUTLET										
0.07	57.3	57.4	57.5	57.5	57.6	57.7	57.8	57.9	57.9	58.0	58.1	58.1	58.1	58.0	58.0	57.9	57.9	57.8	57.8	57.7	57.7	57.6
0.13	56.0	56.0	56.1	56.2	56.3	56.4	56.5	56.5	56.6	56.7	56.8	56.8	56.7	56.7	56.6	56.6	56.5	56.5	56.4	56.4	56.3	56.3
0.20	54.7	54.7	54.8	54.9	55.0	55.1	55.2	55.2	55.3	55.4	55.5	55.5	55.4	55.4	55.3	55.3	55.2	55.2	55.1	55.1	55.0	55.0
0.27	53.5	53.5	53.6	53.7	53.8	53.9	53.9	54.0	54.1	54.2	54.3	54.3	54.2	54.2	54.1	54.1	54.0	54.0	53.9	53.9	53.8	53.8
0.33	51.8	51.8	51.9	52.0	52.1	52.2	52.3	52.4	52.4	52.5	52.6	52.6	52.6	52.5	52.5	52.4	52.4	52.3	52.3	52.2	52.2	52.1
0.40	50.5	50.5	50.6	50.7	50.8	50.9	51.0	51.1	51.1	51.2	51.3	51.3	51.3	51.2	51.2	51.1	51.0	51.0	50.9	50.9	50.8	50.8
0.47	49.2	49.2	49.3	49.4	49.5	49.6	49.7	49.8	49.8	49.9	50.0	50.0	50.0	49.9	49.8	49.8	49.7	49.7	49.6	49.6	49.5	49.5
0.53	47.8	47.8	47.9	48.0	48.1	48.2	48.3	48.4	48.4	48.5	48.6	48.6	48.6	48.5	48.4	48.4	48.3	48.3	48.2	48.2	48.1	48.0
0.60	46.4	46.4	46.5	46.6	46.7	46.8	46.9	47.0	47.0	47.1	47.2	47.2	47.2	47.1	47.0	47.0	46.9	46.9	46.8	46.7	46.7	46.6
0.67	45.7	45.8	45.9	46.0	46.1	46.2	46.3	46.4	46.5	46.5	46.6	46.6	46.6	46.5	46.4	46.3	46.3	46.2	46.1	46.1	46.0	45.9
0.73	45.2	45.3	45.5	45.6	45.8	45.9	46.0	46.1	46.2	46.2	46.3	46.3	46.2	46.1	46.1	46.0	45.9	45.8	45.7	45.6	45.5	45.5
0.80	44.4	44.6	44.8	45.0	45.2	45.3	45.5	45.6	45.7	45.9	46.0	46.0	45.9	45.7	45.6	45.5	45.4	45.3	45.2	45.1	45.0	44.9
0.87	43.9	44.1	44.3	44.5	44.7	44.9	45.1	45.2	45.4	45.5	45.6	45.6	45.5	45.4	45.2	45.1	45.0	44.9	44.7	44.6	44.5	44.4
0.93	43.4	43.6	43.8	44.0	44.2	44.4	44.6	44.8	45.0	45.1	45.3	45.3	45.1	44.9	44.8	44.6	44.5	44.3	44.2	44.0	43.9	43.7
1.00	42.4	42.6	42.9	43.2	43.5	43.7	43.9	44.1	44.3	44.5	44.7	44.7	44.5	44.3	44.1	43.9	43.8	43.6	43.4	43.2	43.0	42.8
	GAS OUTLET											AIR INLET										

Figure F.6.- Metal elements temperature profiles (ºC) for convection-condensation heat transfer with 100% condensed water drainage.

x/L	GAS INLET												AIR OUTLET											
0.07	0	0	0	0	0	0	0	0	0	0	0	0	0	0	0	0	0	0	0	0	0	0	0	0
0.13	0	0	0	0	0	0	0	0	0	0	0	0	0	0	0	0	0	0	0	0	0	0	0	0
0.20	0	0	0	0	0	0	0	0	0	0	0	0	0	0	0	0	0	0	0	0	0	0	0	0
0.27	0	0	0	0	0	0	0	0	0	0	0	0	0	0	0	0	0	0	0	0	0	0	0	0
0.33	0	0	0	0	0	0	0	0	0	0	0	0	0	0	0	0	0	0	0	0	0	0	0	0
0.40	0	0	0	0	0	0	0	0	0	0	0	0	0	0	0	0	0	0	0	0	0	0	0	0
0.47	0	0	0	0	0	0	0	0	0	0	0	0	0	0	0	0	0	0	0	0	0	0	0	0
0.53	0	0	0	0	0	0	0	0	0	0	0	0	0	0	0	0	0	0	0	0	0	0	0	0
0.60	0	0	0	0	0	0	0	0	0	0	0	0	0	0	0	0	0	0	0	0	0	0	0	0
0.67	0.7	0.7	0.5	0.3	0.2	0.0	0	0	0	0	0	0	0	0	0	0	0	0	0	0	0	0	0	0
0.73	1.2	1.2	1.0	0.8	0.7	0.5	0.4	0.3	0.1	0.0	0	0	0	0	0	0	0	0	0	0	0	0	0	0
0.80	2.0	1.9	1.7	1.5	1.3	1.2	1.0	0.8	0.7	0.6	0.5	0.4	0	0	0	0	0	0	0	0	0	0	0	0
0.87	2.2	2.1	1.9	1.8	1.6	1.5	1.3	1.2	1.1	0.9	0.9	0.8	0	0	0	0	0	0	0	0	0	0	0	0
0.93	2.3	2.3	2.1	2.0	1.9	1.8	1.6	1.5	1.4	1.2	1.2	1.1	0	0	0	0	0	0	0	0	0	0	0	0
1.00	3.0	2.9	2.8	2.6	2.5	2.3	2.2	2.0	1.9	1.7	1.7	1.6	0	0	0	0	0	0	0	0	0	0	0	0
	GAS OUTLET												AIR INLET											

Figure F.7.- Condensed/Evaporated (-ve) water flow rate (mol/s) for convection-condensation heat transfer with 100% condensed water drainage.

x/L	GAS INLET												AIR OUTLET											
0.00	1.0	1.0	1.0	1.0	1.0	1.0	1.0	1.0	1.0	1.0	1.0	1.0	1.0	1.0	1.0	1.0	1.0	1.0	1.0	1.0	1.0	1.0	1.0	1.0
0.07	1.0	1.0	1.0	1.0	1.0	1.0	1.0	1.0	1.0	1.0	1.0	1.0	1.0	1.0	1.0	1.0	1.0	1.0	1.0	1.0	1.0	1.0	1.0	1.0
0.13	1.0	1.0	1.0	1.0	1.0	1.0	1.0	1.0	1.0	1.0	1.0	1.0	1.0	1.0	1.0	1.0	1.0	1.0	1.0	1.0	1.0	1.0	1.0	1.0
0.20	1.0	1.0	1.0	1.0	1.0	1.0	1.0	1.0	1.0	1.0	1.0	1.0	1.0	1.0	1.0	1.0	1.0	1.0	1.0	1.0	1.0	1.0	1.0	1.0
0.27	1.0	1.0	1.0	1.0	1.0	1.0	1.0	1.0	1.0	1.0	1.0	1.0	1.0	1.0	1.0	1.0	1.0	1.0	1.0	1.0	1.0	1.0	1.0	1.0
0.33	1.0	1.0	1.0	1.0	1.0	1.0	1.0	1.0	1.0	1.0	1.0	1.0	1.0	1.0	1.0	1.0	1.0	1.0	1.0	1.0	1.0	1.0	1.0	1.0
0.40	1.0	1.0	1.0	1.0	1.0	1.0	1.0	1.0	1.0	1.0	1.0	1.0	1.0	1.0	1.0	1.0	1.0	1.0	1.0	1.0	1.0	1.0	1.0	1.0
0.47	1.0	1.0	1.0	1.0	1.0	1.0	1.0	1.0	1.0	1.0	1.0	1.0	1.0	1.0	1.0	1.0	1.0	1.0	1.0	1.0	1.0	1.0	1.0	1.0
0.53	1.0	1.0	1.0	1.0	1.0	1.0	1.0	1.0	1.0	1.0	1.0	1.0	1.0	1.0	1.0	1.0	1.0	1.0	1.0	1.0	1.0	1.0	1.0	1.0
0.60	1.0	1.0	1.0	1.0	1.0	1.0	1.0	1.0	1.0	1.0	1.0	1.0	1.0	1.0	1.0	1.0	1.0	1.0	1.0	1.0	1.0	1.0	1.0	1.0
0.67	1.7	1.6	1.4	1.4	1.2	1.1	1.0	1.0	1.0	1.0	1.0	1.0	1.0	1.0	1.0	1.0	1.0	1.0	1.0	1.0	1.0	1.0	1.0	1.0
0.73	2.3	2.2	2.0	2.0	1.8	1.7	1.5	1.4	1.2	1.1	1.0	1.0	1.0	1.0	1.0	1.0	1.0	1.0	1.0	1.0	1.0	1.0	1.0	1.0
0.80	3.2	3.1	3.0	2.9	2.7	2.5	2.3	2.1	2.0	1.8	1.6	1.5	1.0	1.0	1.0	1.0	1.0	1.0	1.0	1.0	1.0	1.0	1.0	1.0
0.87	3.7	3.7	3.5	3.4	3.3	3.1	2.9	2.8	2.6	2.4	2.2	2.1	1.0	1.0	1.0	1.0	1.0	1.0	1.0	1.0	1.0	1.0	1.0	1.0
0.93	4.2	4.1	4.0	4.0	3.9	3.7	3.5	3.4	3.2	3.1	2.9	2.8	1.0	1.0	1.0	1.0	1.0	1.0	1.0	1.0	1.0	1.0	1.0	1.0
1.00	5.0	5.0	4.9	4.8	4.7	4.6	4.4	4.3	4.2	4.0	3.8	3.7	1.0	1.0	1.0	1.0	1.0	1.0	1.0	1.0	1.0	1.0	1.0	1.0
	GAS OUTLET												AIR INLET											

Figure F.8.- Augmentation factors for convection-condensation heat transfer with 100% condensed water drainage.